Angewandte
Eine Zeitschrift der Gesellschaft Deutscher Chemiker
Chemie

Supporting Information

Morphological Control of Heteroleptic *cis*- and *trans*-$Pd_2L_2L'_2$ Cages

*Witold M. Bloch, Julian J. Holstein, Wolf Hiller, and Guido H. Clever**

anie_201702573_sm_miscellaneous_information.pdf

Supporting information

Contents

1. Experimental Section

1.1. Materials and measurements

Unless otherwise stated, all chemicals were obtained from commercial sources and used as received. Ligands $\mathbf{L^A}$, $\mathbf{L^P}$ and $\mathbf{L^C}$ (scheme S1) were prepared according to literature procedures.[1,2] Electrospray ionization (ESI) mass spectra were recorded on a Bruker Apex IV ESI-FTICR Mass Spectrometer with a dual electrospray ionization source. GPC purification of ligand **L** was performed on a JASCO LC-9210 II NEXT.

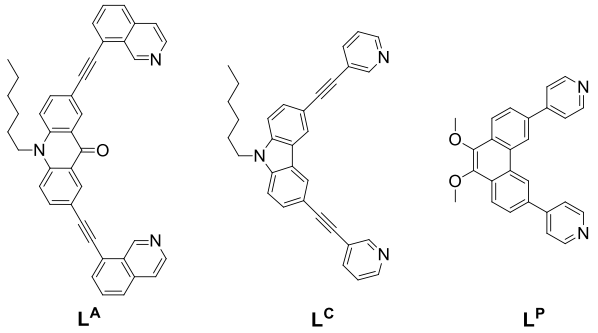

Scheme S1

1.2. Synthesis of homoleptic cages

The synthesis of Pd(II) cages from $\mathbf{L^A}$ and $\mathbf{L^P}$ were investigated in CD_3CN. The assembly of the cages $[Pd_2\mathbf{L^A}_4]^{4+}$ and $[Pd_4\mathbf{L^P}_8]^{8+}$ has previously been described in DMSO.[1]

1.2.1. Synthesis of $[Pd_2\mathbf{L^A}_4]^{4+}$

A solution of $[Pd(CH_3CN)_4](BF_4)_2$ (60.0 µL, 15 mM/CD_3CN, 0.9 µmol) was combined with a suspension of $\mathbf{L^A}$ (1.0 mg, 1.7 µmol) in CD_3CN (540 µL) and heated at 70 °C for 2 h to afford $[Pd_2\mathbf{L^A}_4]^{4+}$ in quantitative yield. ^{1}H NMR (500 MHz, CD_3CN) δ 9.50 (s, 8H, H_i), 8.44 (s, 8H, H_c), 8.33 (d, J = 6.5 Hz, 8H, H_h), 8.02 (d, J = 7.8 Hz, 8H, H_f), 7.94 (d, J = 6.5 Hz, 8H, H_g), 7.89 (t, J = 7.8 Hz, 8H, H_e), 7.74 (d, J = 7.8 Hz, 8H, H_d), 7.42 (d, J = 9.0 Hz, 8H, H_b), 7.19 (d, J = 9.0 Hz, 8H, H_a), 4.42 – 4.10 (m, 8H, CH_2), 1.85 – 1.74 (m, 8H, CH_2), 1.66 – 1.51 (m, 8H, CH_2), 1.51 – 1.29 (m, 16H, 2 x CH_2), 0.93 (t, J = 7.1 Hz, 12H, CH_3).

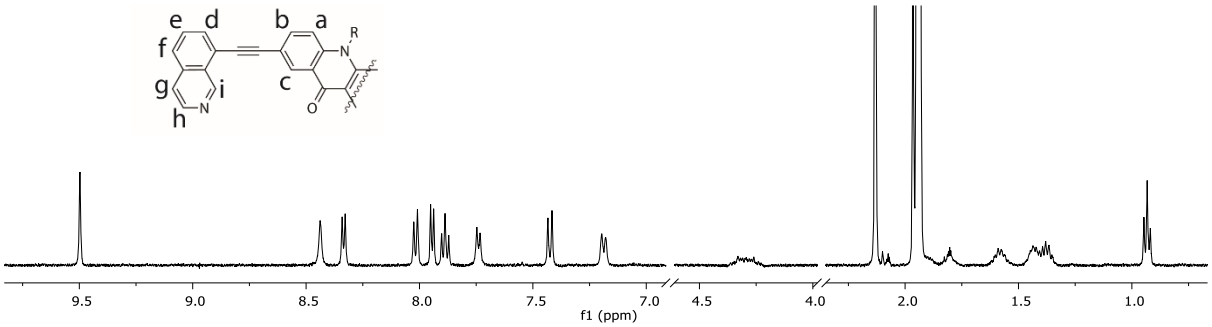

Figure S1. Partial ^{1}H NMR spectrum (500 MHz/CD_3CN) of $[Pd_2\mathbf{L^A}_4]^{4+}$. R = C_6H_{13}.

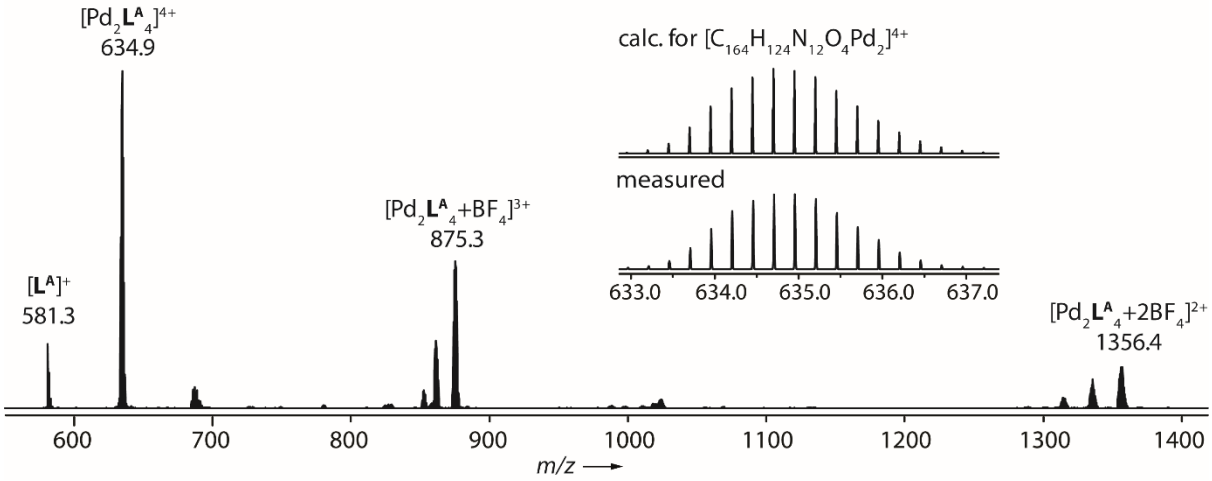

Figure S2. HR ESI-MS spectrum of $[Pd_2\mathbf{L^A}_4]^{4+}$ (prepared in CD_3CN). The calculated and theoretical pattern of $[Pd_2\mathbf{L^A}_4]^{4+}$ is shown in the inset.

1.2.2. Synthesis of $[Pd_3\mathbf{L}^{\mathbf{P}}{}_6]^{6+}$ / $[Pd_4\mathbf{L}^{\mathbf{P}}{}_8]^{8+}$

A solution of $[Pd(CH_3CN)_4](BF_4)_2$ (60.0 µL, 15 mM/CD_3CN, 0.9 µmol) was combined with a solution of $\mathbf{L}^{\mathbf{P}}$ (0.67 mg, 1.7 µmol) in CD_3CN (540 µL) and heated at 70 °C for 2 h to afford a 1:2 mixture of $[Pd_3\mathbf{L}^{\mathbf{P}}{}_6]^{6+}$ / $[Pd_4\mathbf{L}^{\mathbf{P}}{}_8]^{8+}$ in quantitative yield. ^{1}H NMR (500 MHz, CD_3CN, 60 °C) δ 9.50 (s, 32H, $H_{e'}$), 9.32 (s, 12H, H_c), 9.17 (d, J = 6.5 Hz, 24H, H_e), 9.10 (s, 16H, $H_{c'}$), 8.40 (s, br, 16H, $H_{a'}$), 8.37 (d, J = 8.7 Hz, 12H, H_a), 8.31 (d, J = 6.5 Hz, 24H, H_d), 8.27 (s, 32H, $H_{d'}$), 8.11 (d, J = 8.7 Hz, 12H, H_b), 7.95 (s, 16H, $H_{b'}$), 4.09 (s, 36 + 48H, OMe/OMe').

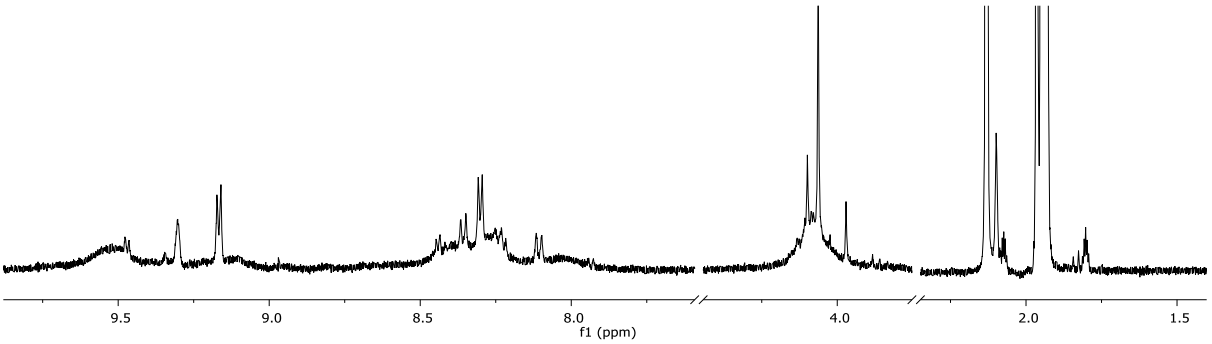

Figure S3. Partial ^{1}H NMR spectrum (500 MHz/CD_3CN, 25 °C) of the mixture of $[Pd_3\mathbf{L}^{\mathbf{P}}{}_6]^{6+}$ and $[Pd_4\mathbf{L}^{\mathbf{P}}{}_8]^{8+}$.

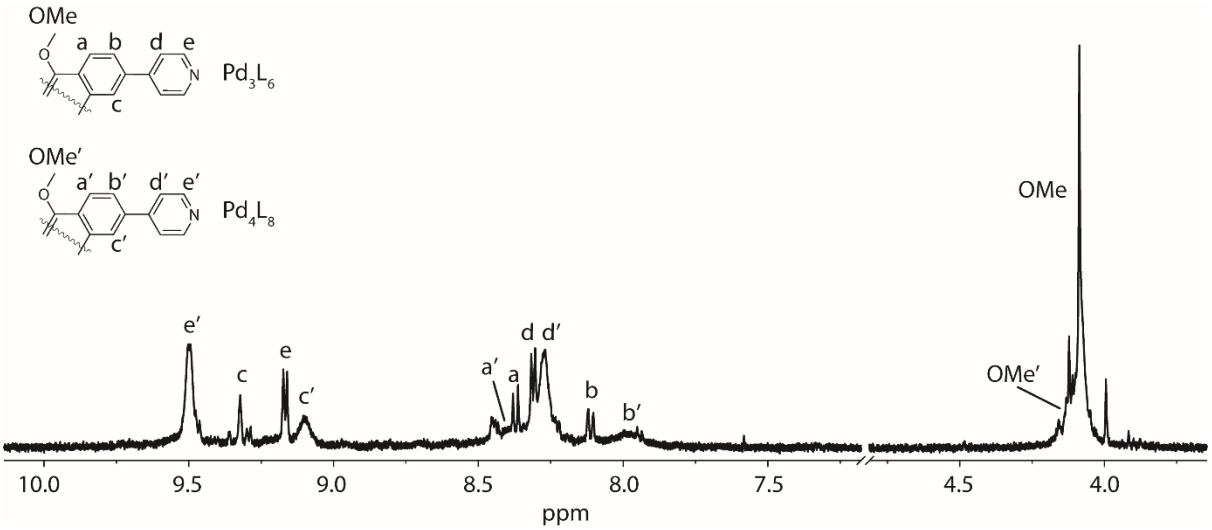

Figure S4. Partial ^{1}H NMR spectrum (500 MHz/CD_3CN, 60 °C) of the mixture of $[Pd_3\mathbf{L}^{\mathbf{P}}{}_6]^{6+}$ and $[Pd_4\mathbf{L}^{\mathbf{P}}{}_8]^{8+}$. The ratio of these two species is approximately 1:2 respectively (calculated from the relative ^{1}H NMR signals of each structure, taking into account the ligand/metal stoichiometries). The other minor signals may to be due to a tetrahedral isomer of the $[Pd_4\mathbf{L}^{\mathbf{P}}{}_8]^{8+}$ species.[3]

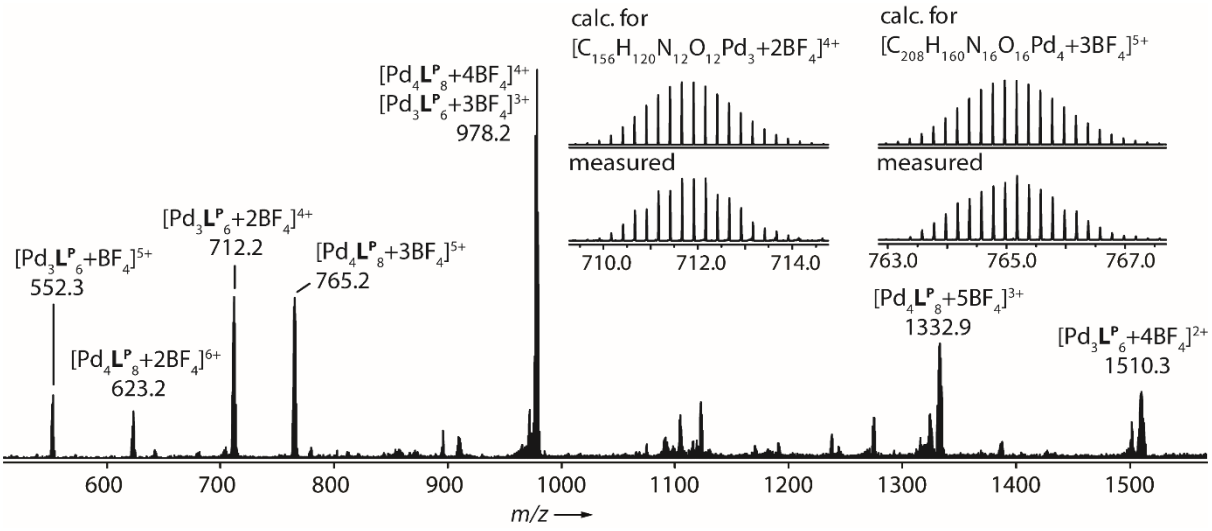

Figure S5. ESI mass spectrum of the mixture of $[Pd_3\mathbf{L}^{\mathbf{P}}{}_6]^{6+}$ and $[Pd_4\mathbf{L}^{\mathbf{P}}{}_8]^{8+}$ (prepared in CD_3CN). The measured and calculated pattern for $[Pd_3\mathbf{L}^{\mathbf{P}}{}_6 + 2BF_4]^{4+}$ and $[Pd_4\mathbf{L}^{\mathbf{P}}{}_8 + 3BF_4]^{5+}$ are shown in the inset.

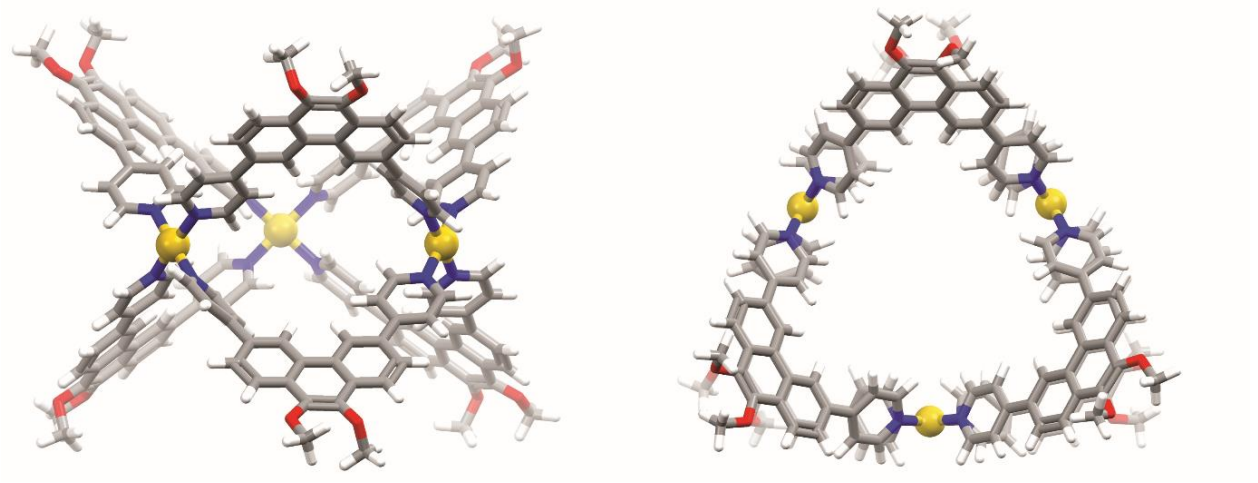

Figure S6. PM6 model of $[Pd_3\mathbf{L^P}_6]^{6+}$ calculated using Gaussian 09.[4] The presence of the species $[Pd_3\mathbf{L^P}_6]^{6+}$ in CD_3CN and not DMSO[1] is presumably due to solvent effects.[5]

1.3. Synthesis of heteroleptic cages

*1.3.1. Synthesis of cis-$[Pd_2\mathbf{L^A}_2\mathbf{L^P}_2]^{4+}$ (**1**)*

1 was prepared in a similar fashion as previously described. A solution of $[Pd(CH_3CN)_4](BF_4)_2$ (120 µL, 15 mM/CD_3CN, 1.80 µmol) was combined with a suspension of $\mathbf{L^A}$ (1.00 mg, 1.72 µmol) and $\mathbf{L^P}$ (0.67 mg, 1.72 µmol) in CD_3CN (300 µL) and heated at 70 °C for 24 h to afford $[Pd_2\mathbf{L^A}_2\mathbf{L^P}_2]^{4+}$ (**1**) in >99% yield. ^{1}H NMR (500 MHz/CD_3CN, 25 °C): δ 10.39 (s, 4H, H_i), 9.36 – 9.07 (m, 16H, $H_{c'}$, $H_{e'}$, H_h), 8.63 (s, 4H, H_c), 8.33 (d, J = 8.7 Hz, 4H, $H_{a'}$), 8.27 (d, J = 6.1 Hz, 8H, $H_{d'}$), 8.08 (d, J = 6.5 Hz, 4H, H_g), 8.03 – 7.94 (m, 12H, $H_{b'}$, H_f, H_d), 7.91 – 7.80 (m, 8H, H_e, H_b), 7.43 (s, 4H, H_a), 4.06 (s, 12H, OMe), 1.73 (s, 4H, CH_2), 1.53 (s, 4H, CH_2), 1.38 (s, 8H, 2 x CH_2), 0.93 (s, 6H, CH_3).

^{1}H NMR (500 MHz/CD_3CN, 60 °C): δ 10.29 (s, 4H, H_i), 9.29 – 9.20 (m, 12H, $H_{e'}$, $H_{c'}$), 9.07 (d, J = 6.5 Hz, 4H, H_h), 8.66 (d, J = 2.1 Hz, 4H, H_c), 8.33 (d, J = 8.7 Hz, 4H, $H_{a'}$), 8.29 – 8.24 (m, 8H, $H_{d'}$), 8.09 (d, J = 6.5 Hz, 4H, H_g), 8.04 – 7.96 (m, 12H, $H_{b'}$, h_f, H_d), 7.90 (dd, J = 8.5, 7.0 Hz, 4H, H_e), 7.83 (dd, J = 8.9, 2.1 Hz, 4H, H_b), 7.43 (d, J = 8.9 Hz, 4H, H_a), 4.16 – 4.10 (m, 4H, CH_2), 4.09 (s, 12H, OMe), 1.78 – 1.70 (m, 4H, CH_2), 1.57 – 1.48 (m, 4H), 1.44 – 1.30 (m, 8H), 0.93 (t, J = 7.1 Hz, 6H).

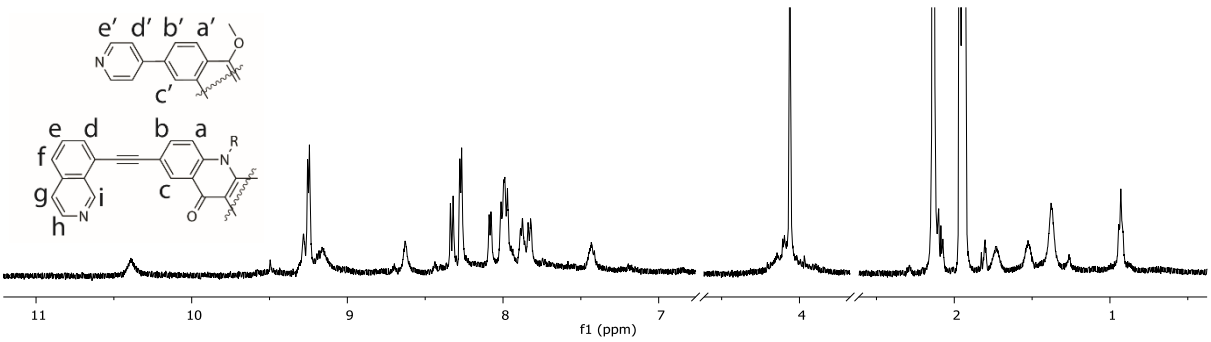

Figure S7. Partial ^{1}H NMR spectrum (500 MHz/CD_3CN/25 °C) of *cis*-$[Pd_2\mathbf{L^A}_2\mathbf{L^P}_2]^{4+}$ (**1**). For $\mathbf{L^A}$, R = C_6H_{13}.

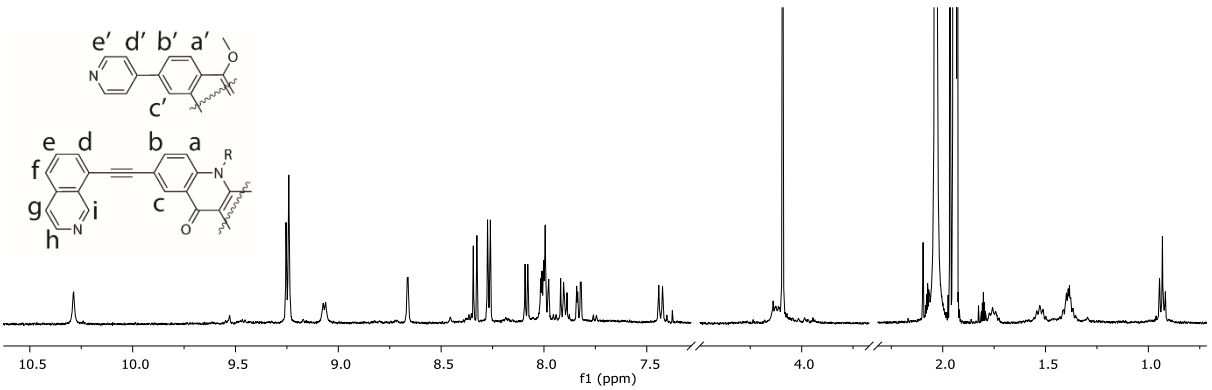

Figure S8. Partial ^{1}H NMR spectrum (500 MHz/CD_3CN/60 °C) of *cis*-$[Pd_2\mathbf{L^A}_2\mathbf{L^P}_2]^{4+}$ (**1**). For $\mathbf{L^A}$, R = C_6H_{13}.

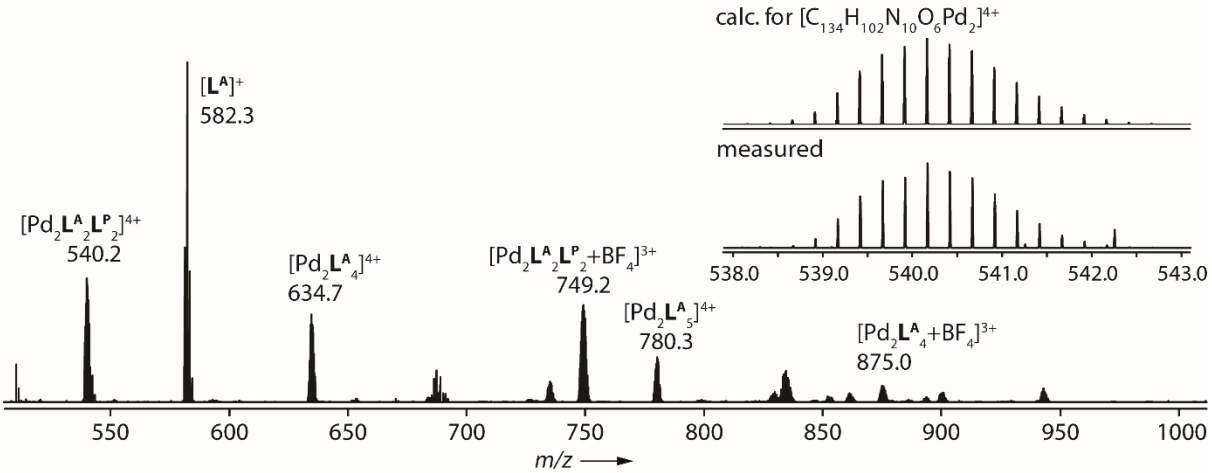

Figure S9. ESI mass spectrum of $[Pd_2\mathbf{L^A}_2\mathbf{L^P}_2]^{4+}$ (**1**) (prepared in CD_3CN). The measured and calculated pattern for $[Pd_2\mathbf{L^A}_2\mathbf{L^P}_2]^{4+}$ is shown in the inset.

*1.3.2. Synthesis of cis-$[Pd_2\mathbf{L^C}_2\mathbf{L^P}_2]^{4+}$ (**2**)*

A solution of $[Pd(CH_3CN)_4](BF_4)_2$ (60.0 µL, 15 mM/CD_3CN 0.9 µmol) was combined with a solution of $\mathbf{L^C}$ (120 µL, 7 mM/CD_3CN, 1.68 µmol) and $\mathbf{L^P}$ (120 µL, 7 mM/CD_3CN, 1.68 µmol) in CD_3CN (300 µL) and heated at 70 °C for 16 h to afford **2**, *cis*-$[Pd_2\mathbf{L^C}_2\mathbf{L^P}_2]^{4+}$ in >99% yield. ^{1}H NMR (500 MHz, CD_3CN): δ 9.71 (d, *J* = 1.8 Hz, 4H, H_g), 9.32 (s, 4H, $H_{c'}$), 9.15 – 9.07 (m, 12H, $H_{e'}$, H_f), 8.54 (s, 4H, H_c), 8.32 (d, *J* = 8.6 Hz, 4H, $H_{a'}$), 8.29 (d, *J* = 6.2 Hz, 8H, $H_{d'}$), 8.10 (d, *J* = 8.0 Hz, 4H, H_d), 8.07 (d, *J* = 8.6 Hz, 4H, $H_{b'}$), 7.73 – 7.67 (m, 8H, H_e, H_b), 7.58 (d, *J* = 8.5 Hz, 4H, H_a), 4.34 (t, *J* = 7.2, 7.2 Hz, 4H, N-CH_2), 4.04 (s, 12H, 4 x O-CH_3), 1.89 – 1.64 (m, 4H, CH_2), 1.35 – 1.00 (m, 12H, 3 x CH_2), 0.75 (t, *J* = 7.0, 7.0 Hz, 6H, 2 x CH_3). ^{13}C NMR (150 MHz, CD_3CN) δ 172.95, 153.94, 152.45, 151.92, 150.24, 145.93, 142.55 , 142.29 , 133.16 , 131.92 , 131.00 , 129.45 , 128.27 , 126.07 , 125.95 , 125.53 , 124.44 , 123.12 , 112.92 , 111.30 , 97.92 , 83.22 , 79.07, 61.70 , 43.96 , 34.78 , 32.00 , 29.35 , 27.17 , 23.06 . ^{19}F (376 Hz/CD_3CN-d_6): −150.67. ESI-HR-MS ($C_{116}H_{94}N_{10}O_4Pd_4$) calc: 476.1395 [**2**]$^{4+}$, 663.8535 [**2**+$BF_4$]$^{3+}$, 1039.2823 [**2**+2$BF_4$]$^{2+}$; found: 476.1420 [**2**]$^{4+}$, 663.8582 [**2**+BF_4]$^{3+}$, 1039.2912 [**2**+2BF_4]$^{2+}$.

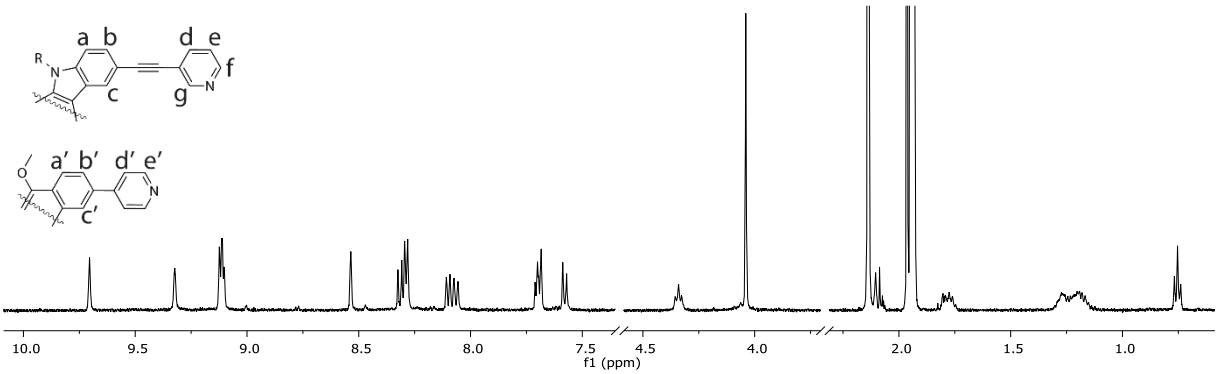

Figure S10. Partial ^{1}H NMR spectrum (500 MHz/CD_3CN) of *cis*-$[Pd_2\mathbf{L^C}_2\mathbf{L^P}_2]^{4+}$ (**2**). R = C_6H_{13}.

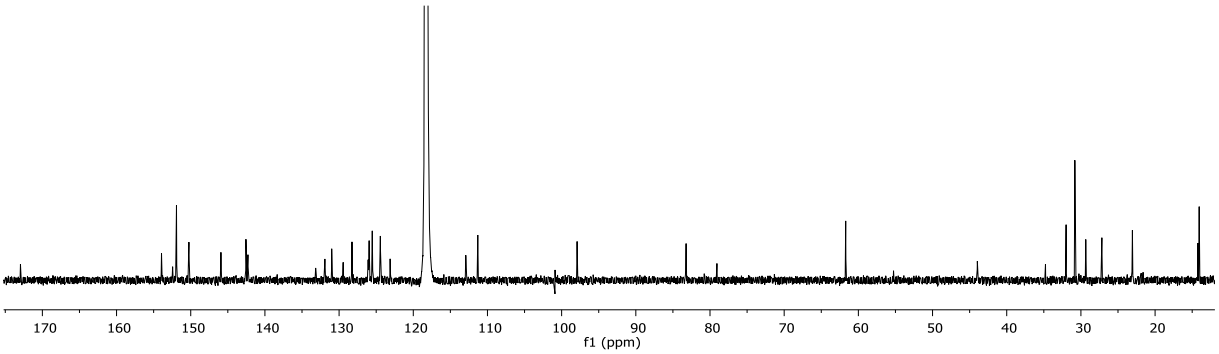

Figure S11. ^{13}C NMR spectrum (150 MHz/CD_3CN) of *cis*-$[Pd_2\mathbf{L}^{C}_2\mathbf{L}^{P}_2]^{4+}$ (**2**).

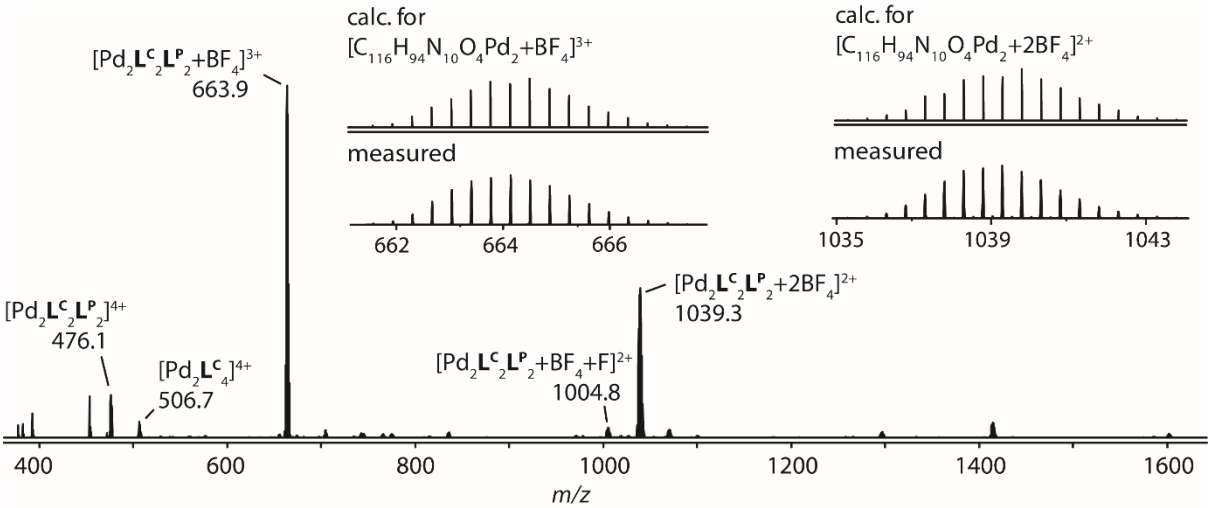

Figure S12. ESI-MS spectrum of *cis*-$[Pd_2\mathbf{L}^{C}_2\mathbf{L}^{P}_2+nBF_4]^{4-n+}$ (**2**) with n = 0–2. The observed and calculated isotope patterns of $[Pd_2\mathbf{L}^{C}_2\mathbf{L}^{P}_2+BF_4]^{3+}$ and $[Pd_2\mathbf{L}^{P}_2\mathbf{L}^{C}_2+2BF_4]^{2+}$ are shown in the inset.

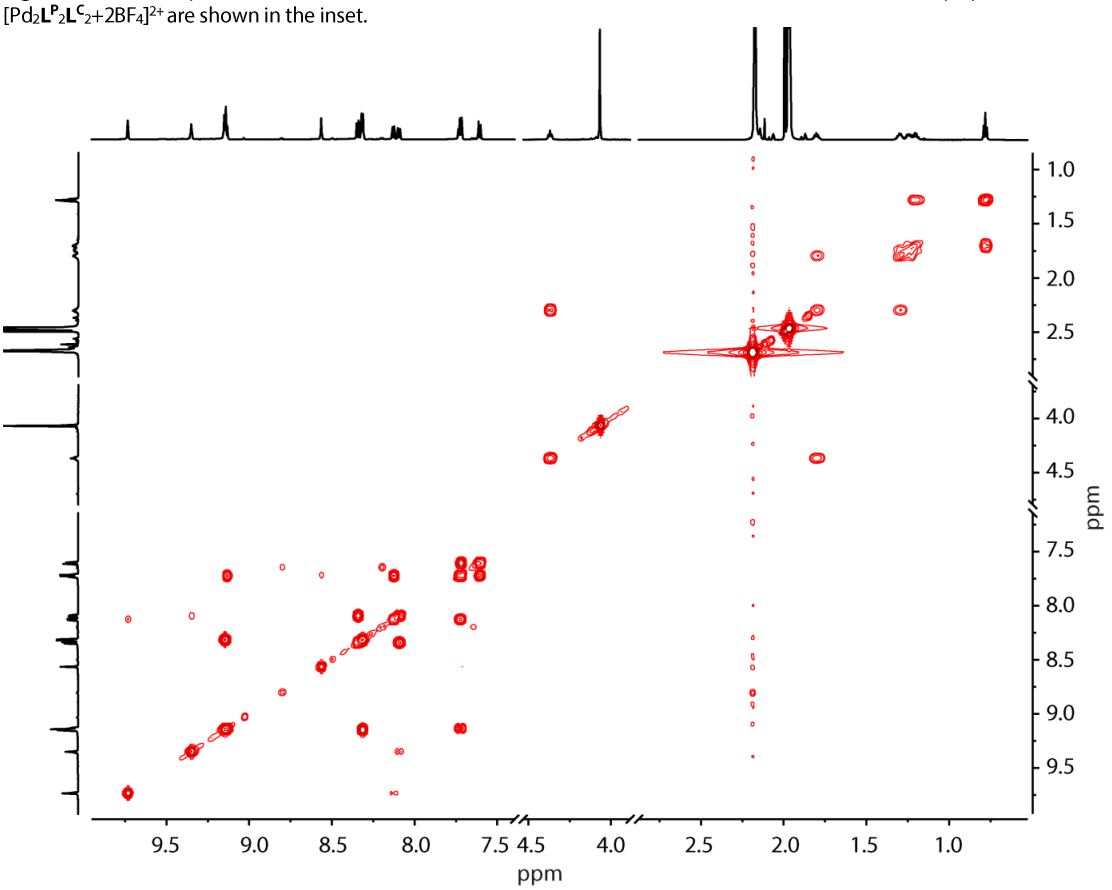

Figure S13. ^{1}H – ^{1}H COSY spectrum (600 MHz/CD_3CN) of *cis*-$[Pd_2\mathbf{L}^{C}_2\mathbf{L}^{P}_2]^{4+}$ (**2**).

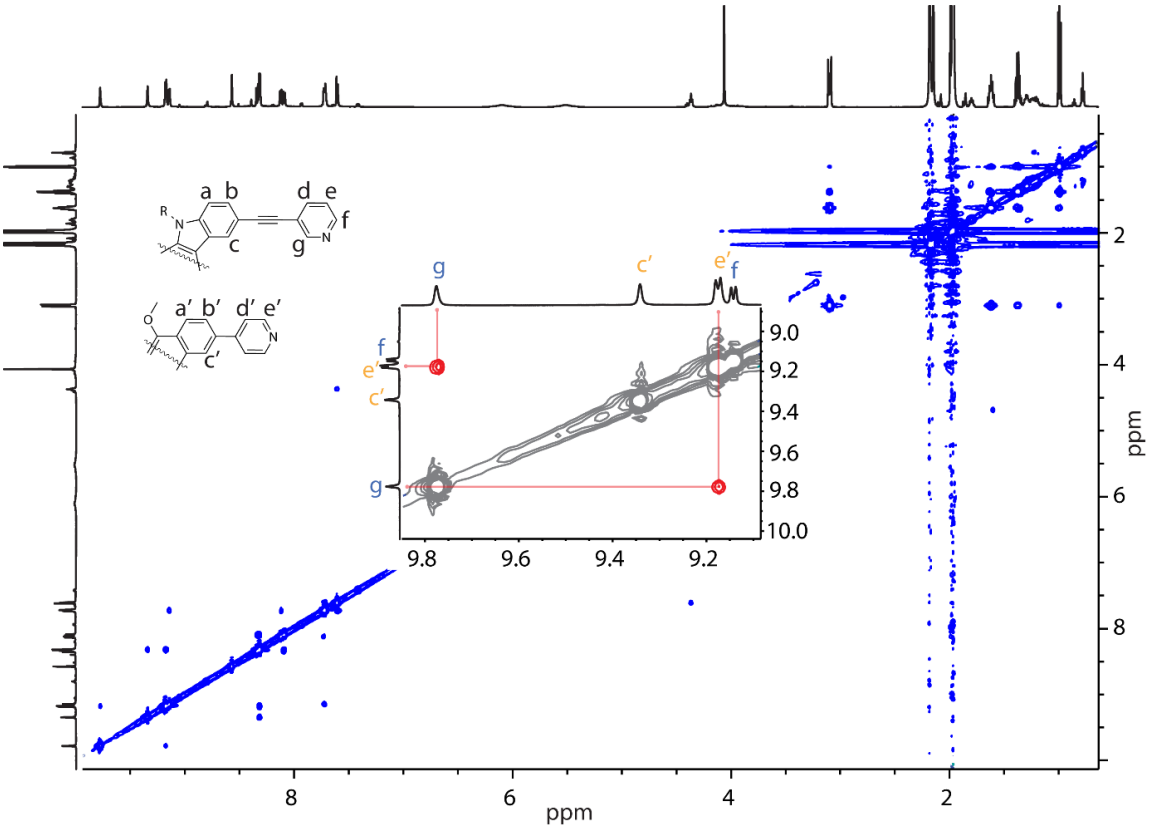

Figure S14. $^{1}H - {}^{1}H$ NOESY spectrum (600 MHz/CD_3CN) of **2** + 2 eq. of F^-. The original NOESY NMR spectrum of **2** did not initially provide clear information of the NOE contacts between $\mathbf{L^C}$ and $\mathbf{L^P}$ due to overlapping of the signals attributed to the inner-pointing protons $H_{e'}$ and H_f. However, these proton signals were observed to shift and separate upon titrating **2** with F^- anions (Figure S23), allowing the inter-ligand NOE contact ($H_{e'} \cdots H_g$) to be clearly visualized in the NOESY experiment. The expansion in the inset shows this inter-ligand contact ($H_{e'} \cdots H_g$), confirming the close proximity of $\mathbf{L^A}$ and $\mathbf{L^P}$ in the cage structure. For $\mathbf{L^C}$, R = C_6H_{13}.

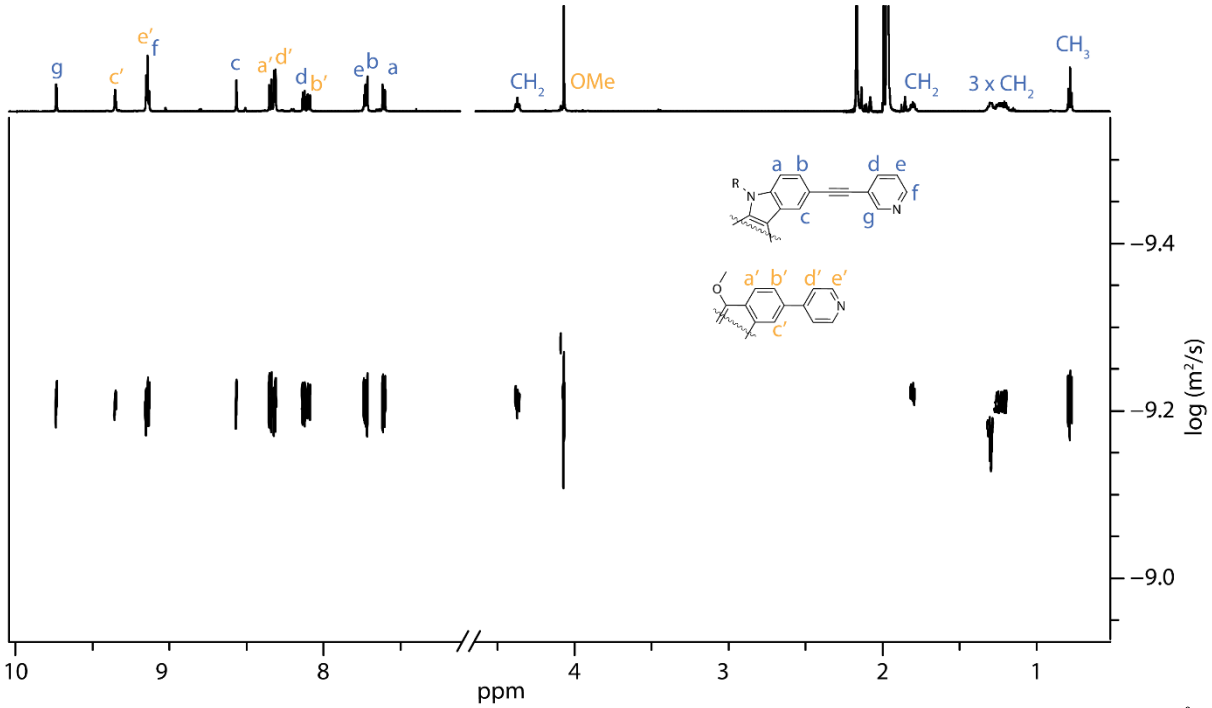

Figure S15. DOSY spectrum (600 MHz, CD_3CN) of **2**. Diffusion coefficient: 6.21 x 10^{-10} m^2s^{-1}, log D = −9.21. Hydrodynamic radius = 9.53 Å. For $\mathbf{L^C}$, R = C_6H_{13}.

*1.3.3. Synthesis of trans-[Pd$_2$(anti-**L^A**)$_2$**L^C**$_2$]$^{4+}$(**3**)*

A solution of [Pd(CH$_3$CN)$_4$](BF$_4$)$_2$ (335 µL, 15 mM/CD$_3$CN 5.0 µmol) was combined with a suspension of **L^A** (2.80 mg, 4.8 µmol) and **L^C** (2.18 mg, 4.8 µmol) in CD$_3$CN (3103 µL) and heated at 70 °C for 16 h to afford *trans*-[Pd$_2$(anti-**L^A**)$_2$**L^C**$_2$]$^{4+}$ (**3**) in 87% yield. ^{1}H NMR (700 MHz, CD$_3$CN) δ 10.48 (s, 2H, H$^A_{i'}$),10.42 (d, *J* = 1.9 Hz, 2H, H$^C_{g'}$), 10.08 (d, *J* = 1.9 Hz, 2H, H^C_g), 10.04 (s, 2H, H^A_i), 9.40 (d, *J* = 2.1 Hz, 2H, H^A_c), 9.25 (d, *J* = 6.2 Hz, 2H, H$^A_{g'}$), 9.15 (d, *J* = 6.2 Hz, 2H, H^A_g), 9.05 (dd, *J* = 6.4, 1.5 Hz, 2H, H^C_f), 8.91 (dd, *J* = 6.4, 1.5 Hz, 2H, H$^C_{f'}$), 8.81 (d, *J* = 2.1 Hz, 2H, H$^A_{c'}$), 8.34 – 8.30 (m, 4H, H$^A_{f'}$, H$^A_{d'}$), 8.29 (dd, *J* = 8.8, 2.2 Hz, 2H, H$^A_{b'}$), 8.27 – 8.23 (m, 4H, H$^A_{h'}$, H$^A_{e'}$), 8.21 (d, *J* = 6.2 Hz, 2H, H^A_h), 8.12 (d, *J* = 8.2 Hz, 2H, H^A_f), 8.05 (dt, *J* = 8.1, 1.5, 1.9 Hz, 2H, H^C_d), 8.01 (dd, *J* = 8.2, 7.0 Hz, 2H, H^A_e), 7.98 (dt, *J* = 7.9, 1.5, 1.9 Hz, 2H, H$^C_{d'}$), 7.92 (dd, *J* = 7.0, 0.9 Hz, 2H, H^A_d), 7.65 – 7.62 (m, 4H, H^A_b,H^C_e), 7.55 (dd, *J* = 7.9, 6.4 Hz, 2H, H$^C_{e'}$), 7.48 (dd, *J* = 8.5, 1.6 Hz, 2H, H^C_b), 7.43 (d, *J* = 8.5 Hz, 2H, H^C_a), 7.23 (d, *J* = 8.4 Hz, 2H, H$^C_{a'}$), 6.96 (d, *J* = 8.4 Hz, 2H, H$^C_{b'}$), 6.91 (d, *J* = 1.5 Hz, 2H, H^C_c), 6.88 (d, *J* = 8.5 Hz, 2H, H^A_a), 6.69 (d, *J* = 1.5 Hz, 2H, H$^C_{c'}$), 6.10 (d, *J* = 8.8 Hz, 2H, H$^A_{a'}$), 4.26 – 4.14 (m, 4H, CH$_2$), 2.50 (s, 2H, CH$_2$), 1.71 (dt, *J* = 13.2, 7.0, 7.0 Hz, 4H, 2 x CH$_2$), 1.34 – 1.16 (m, 14H, 7 x CH$_2$), 1.14 – 1.03 (m, 4H, 2 x CH$_2$), 0.87 (t, *J* = 7.4, 7.4 Hz, 6H, 2 x CH$_3$), 0.82 (t, *J* = 7.0, 7.0 Hz, 6H, 2 x CH$_3$), 0.81 – 0.74 (m, 4H, 2 x CH$_2$) 0.59 (s, 2H, CH$_2$), 0.04 (s, 2H, CH$_2$). ^{19}F (376 Hz/CD$_3$CN): −150.71; ESI-HR-MS (C$_{146}$H$_{116}$N$_{12}$O$_2$Pd$_4$) calc: 570.6862 [**3**]$^{4+}$, 789.9164 [**3**+BF$_4$]$^{3+}$, 1228.3768 [**3**+2BF$_4$]$^{2+}$; found: 570.6875 [**3**]$^{4+}$, 789.9169 [**3**+BF$_4$]$^{3+}$, 1228.3768 [**3**+2BF$_4$]$^{2+}$.

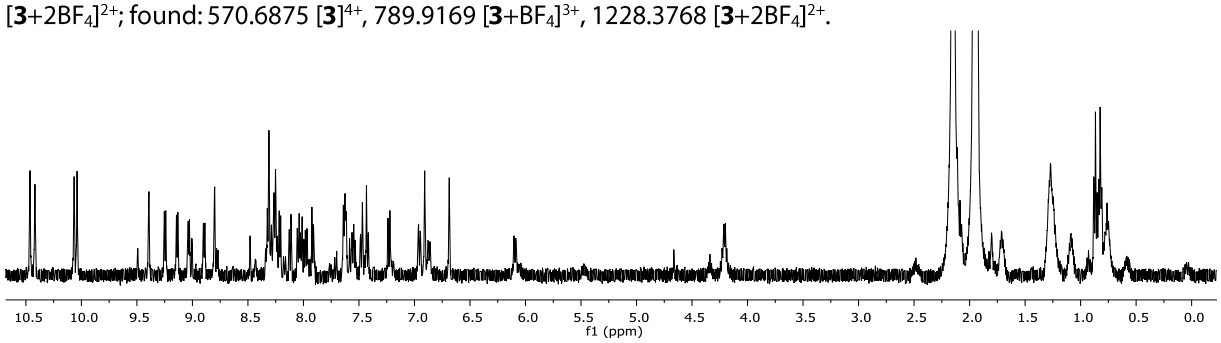

Figure S16. ^{1}H NMR spectrum (500 MHz/CD$_3$CN) of *trans*-[Pd$_2$(*anti*-**L^A**)$_2$**L^C**$_2$]$^{4+}$ (**3**).

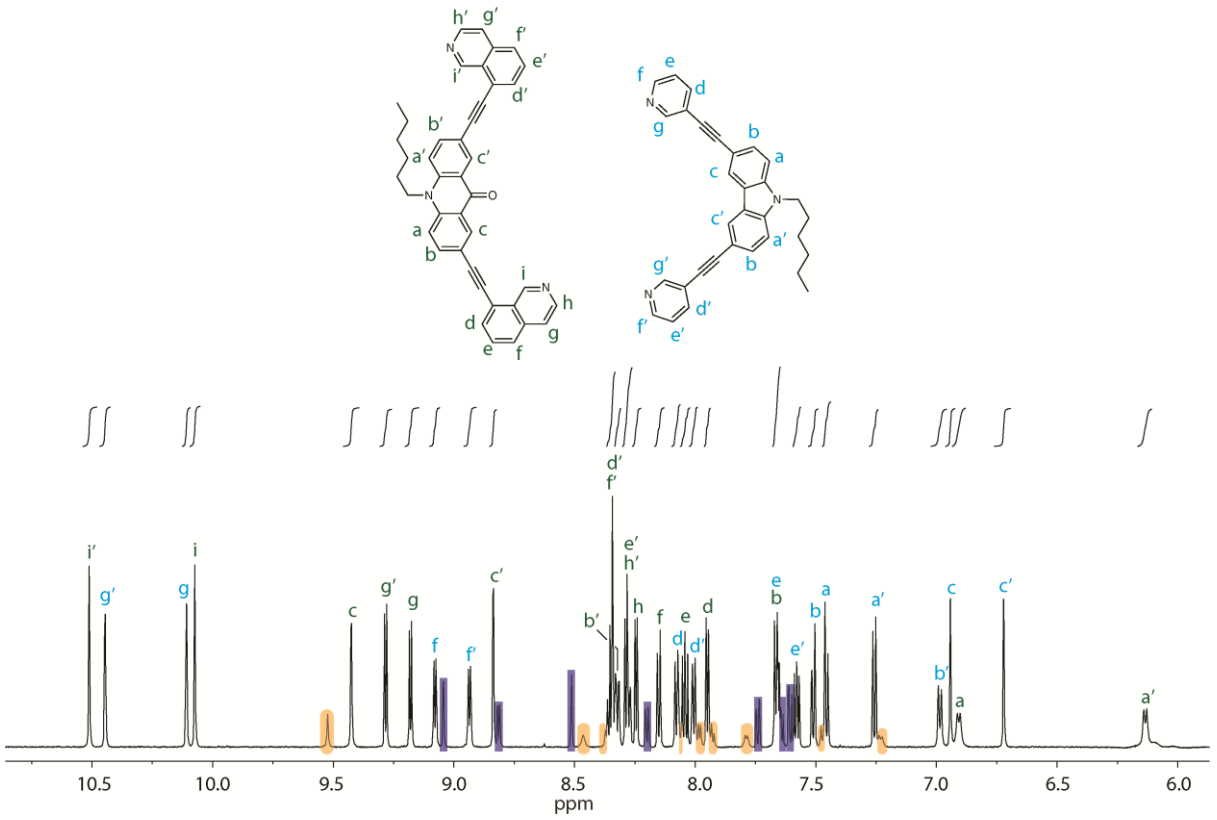

Figure S17. ^{1}H NMR spectrum (700 MHz/CD$_3$CN) of the aromatic region of *trans*-[Pd$_2$(anti-**L^A**)$_2$**L^C**$_2$]$^{4+}$ (**3**) showing integration of the relative aromatic proton signals. The signals highlighted in orange and purple correspond to the homoleptic species [Pd$_2$**L^A**$_4$]$^{4+}$ and [Pd$_2$**L^C**$_4$]$^{4+}$ respectively. Signal assignment was carried out with the aid of COSY and NOESY experiments (see below). Note: efforts to purify **3** by either recrystallization or by precipitation of the homoleptic cages (through the addition of guests) was hindered by its slow re-equilibration into a mixture containing **3** / [Pd$_2$**L^A**$_4$]$^{4+}$ / [Pd$_2$**L^C**$_4$]$^{4+}$ in similar ratios as that observed in the above spectrum.

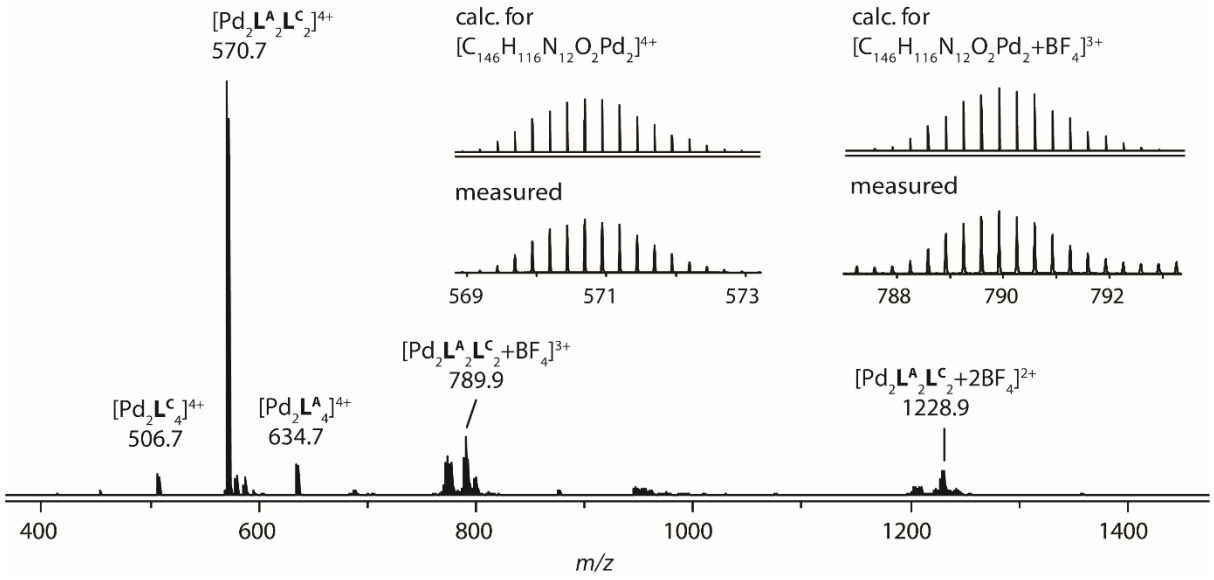

Figure S18. ESI-MS spectrum of *trans*-[Pd_2(anti-$\mathbf{L^A}$)$_2\mathbf{L^C}_2$+nBF_4]$^{4-n+}$ (**3**) with n = 0–2. The observed and calculated isotope patterns of [$Pd_2\mathbf{L^A}_2\mathbf{L^C}_2$]$^{4+}$ and [$Pd_2\mathbf{L^A}_2\mathbf{L^C}_2$+$BF_4$]$^{3+}$ are shown in the inset.

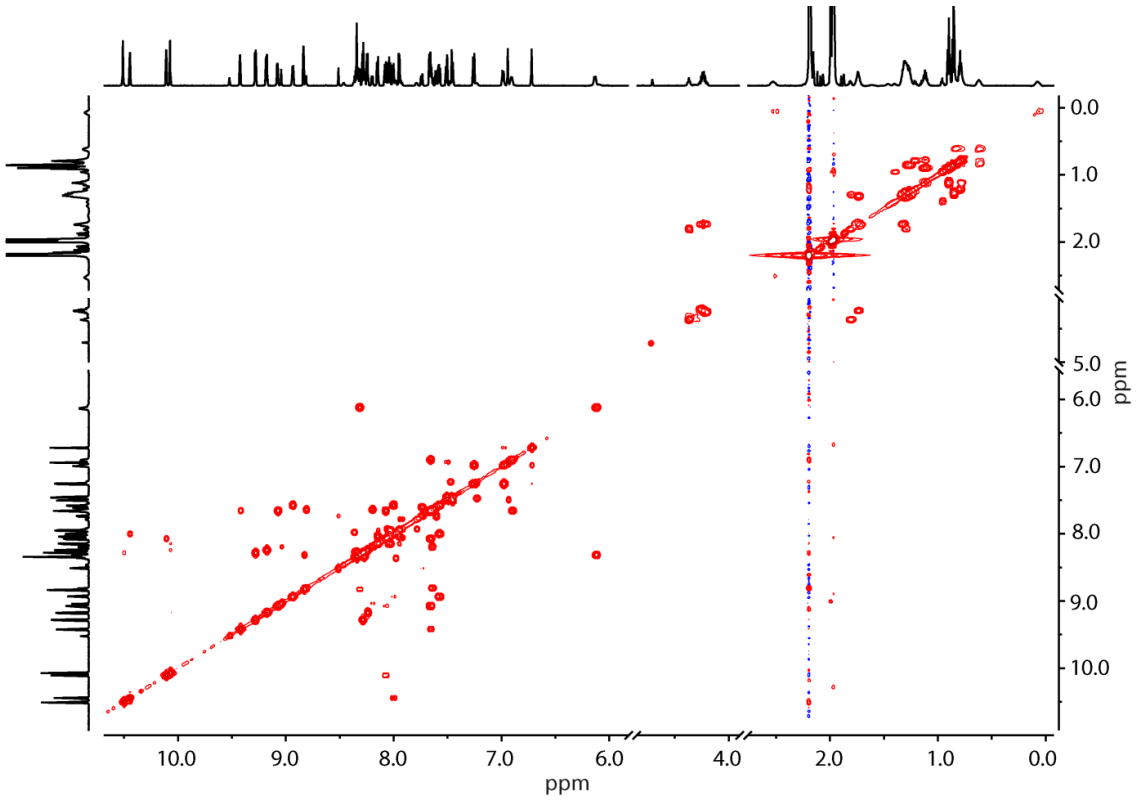

Figure S19. ^{1}H – ^{1}H COSY spectrum (600 MHz/CD_3CN) of *trans*-[Pd_2(anti-$\mathbf{L^A}$)$_2\mathbf{L^C}_2$]$^{4+}$ (**3**).

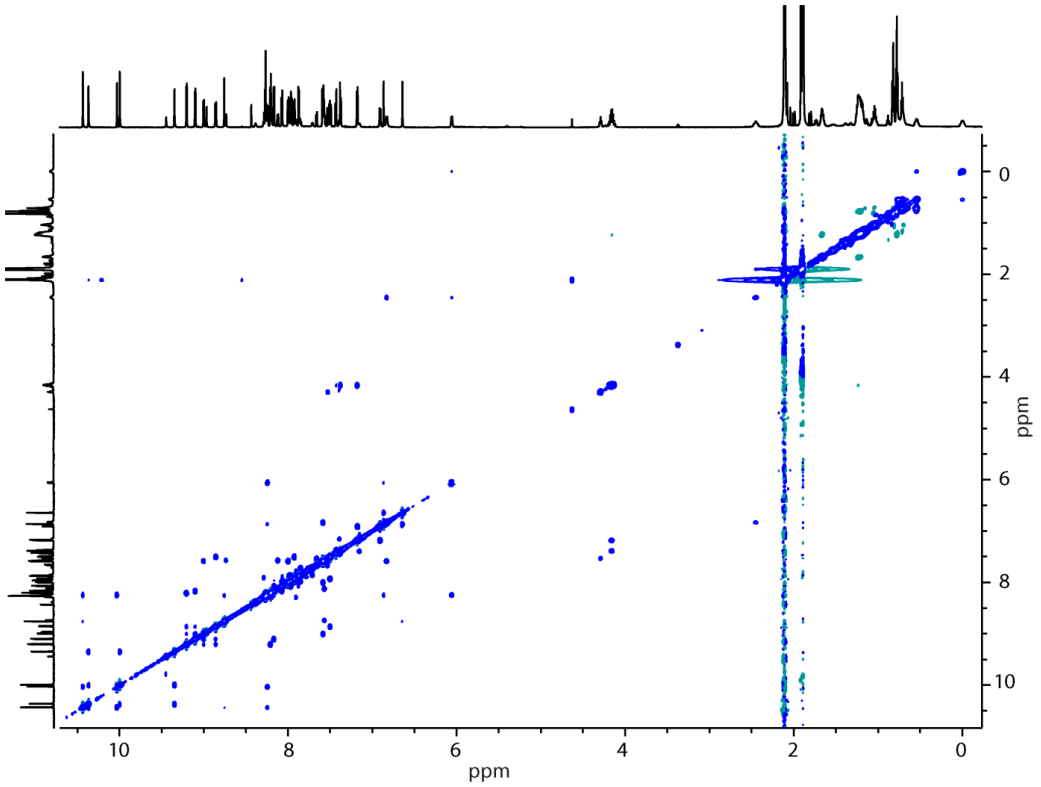

Figure S20. $^{1}H - {}^{1}H$ NOESY spectrum (700 MHz/CD_3CN) of *trans*-$[Pd_2(anti\text{-}\mathbf{L^A})_2\mathbf{L^C}_2]^{4+}$ (**3**).

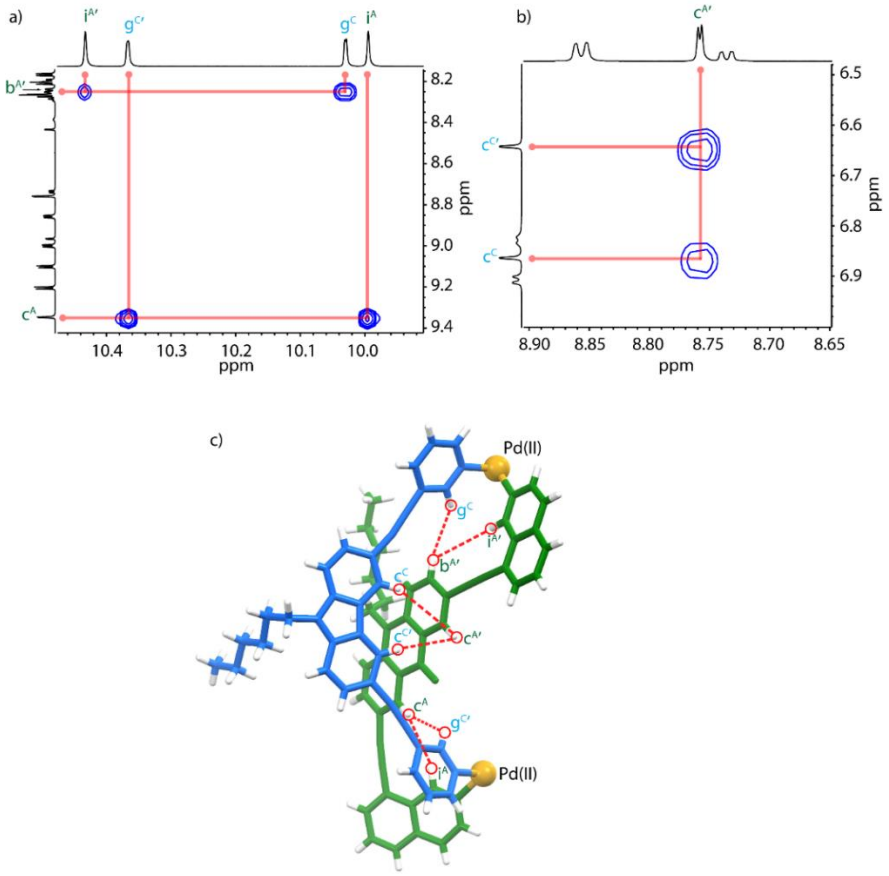

Figure S21. a) and b) expanded regions of the $^{1}H - {}^{1}H$ NOESY spectrum (700 MHz, CD_3CN) of **3**, showing important inter-ligand contacts; c) half of the asymmetric unit of the crystal structure of **3** with contacts between relevant protons shown in red. There is an excellent agreement between the expected contacts from crystal structure and that observed in the NOESY spectrum.

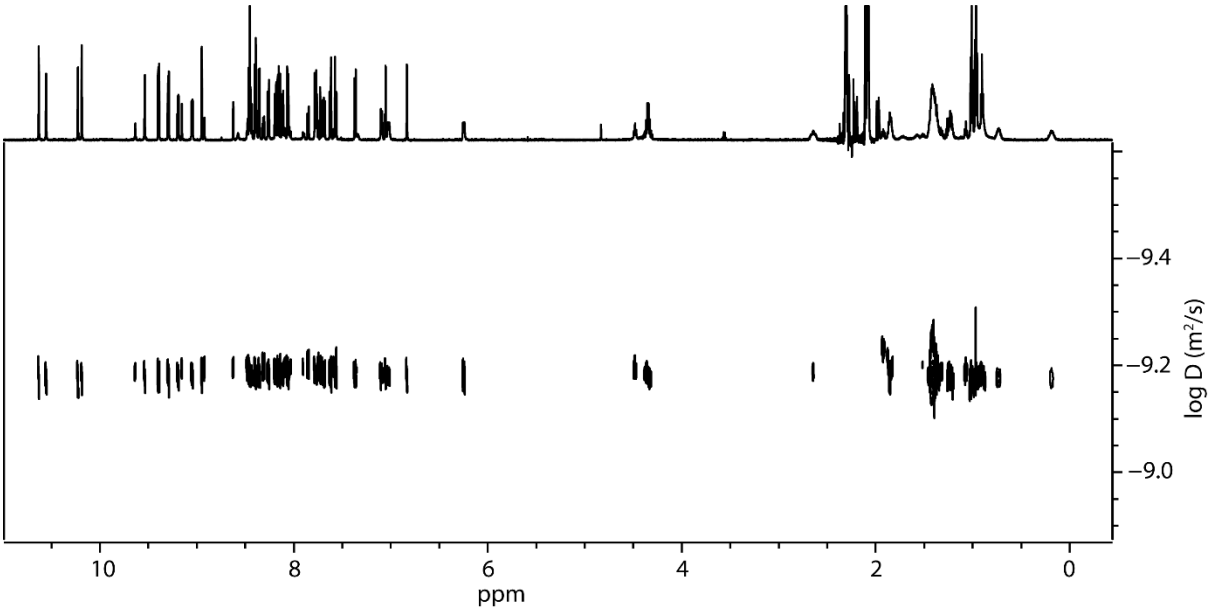

Figure S22. DOSY spectrum (600 MHz, CD_3CN) of **3**. Diffusion coefficient = 6.5 x 10^{-10} m^2s^{-1}, log *D* = −9.19, r = 9.1 Å.

2. Halide titrations

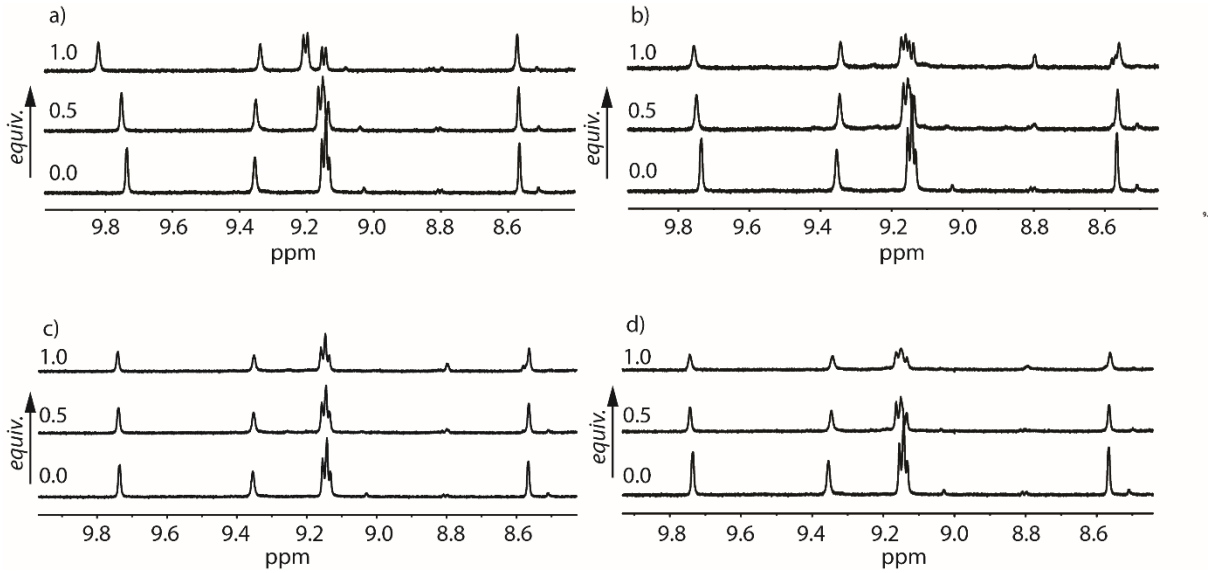

Figure S23. Partial ^{1}H NMR spectra (CD_3CN/500 MHz) showing the stepwise addition of halides ions (tetrabutylammonium salt, 17.5 mM, CD_3CN) to *cis*-$[Pd_2\mathbf{L}^{\mathbf{C}}_2\mathbf{L}^{\mathbf{P}}_2]^{4+}$ (**2**) (0.7 mM, CD_3CN); a) F^-; b) Cl^-; c) Br^-; d) I^-. The amount of halide added (in equivalents) is displayed on the left-hand side of each spectrum. In b) c) and d), the signal rising at 8.8 ppm corresponds to the free ligand due to partial substitution of the halide ions on the Pd(II) centre. The titration with F^- (a) provided a simple deconvolution of signals $H_{e'}$ and H_f. Furthermore, the shifting of proton H_g (9.71 ppm) suggests a weak interaction with F^- inside the cavity of **2**.

3. Cage-to-cage transformations

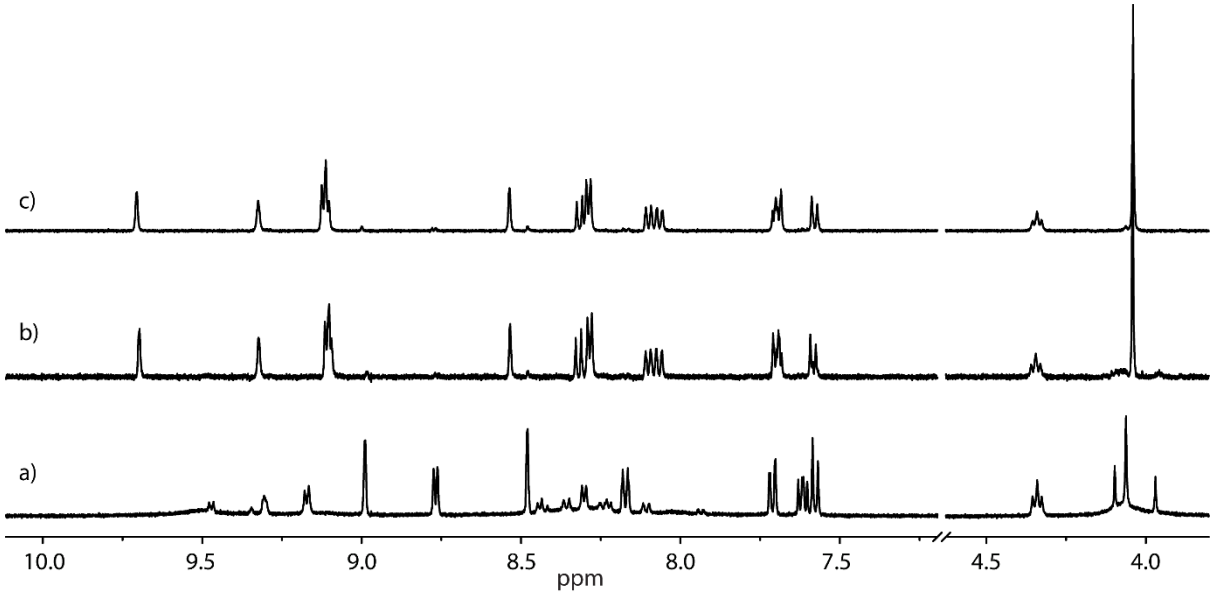

Figure S24. Partial ^{1}H NMR spectra (500 MHz/CD_3CN): a) 2:1 mixture of $[Pd_2\mathbf{L}^{\mathbf{C}}{}_4]^{4+}$ and $[Pd_3\mathbf{L}^{\mathbf{P}}{}_6]^{6+}$ / $[Pd_4\mathbf{L}^{\mathbf{P}}{}_8]^{8+}$; b) 2:1 mixture of $[Pd_2\mathbf{L}^{\mathbf{C}}{}_4]^{4+}$ and $[Pd_3\mathbf{L}^{\mathbf{P}}{}_6]^{6+}$ / $[Pd_4\mathbf{L}^{\mathbf{P}}{}_8]^{8+}$ heated at 70°C for 24 h; c) *cis*-$[Pd_2(\mathbf{L}^{\mathbf{C}})_4\mathbf{L}^{\mathbf{P}}{}_2]^{4+}$ (**2**) obtained by heated a 1:1:1 mixture of $\mathbf{L}^{\mathbf{C}}$, $\mathbf{L}^{\mathbf{P}}$ and $[Pd(CH_3CN)_4](BF_4)_2$ at 70 °C for 24 h, shown for comparison.

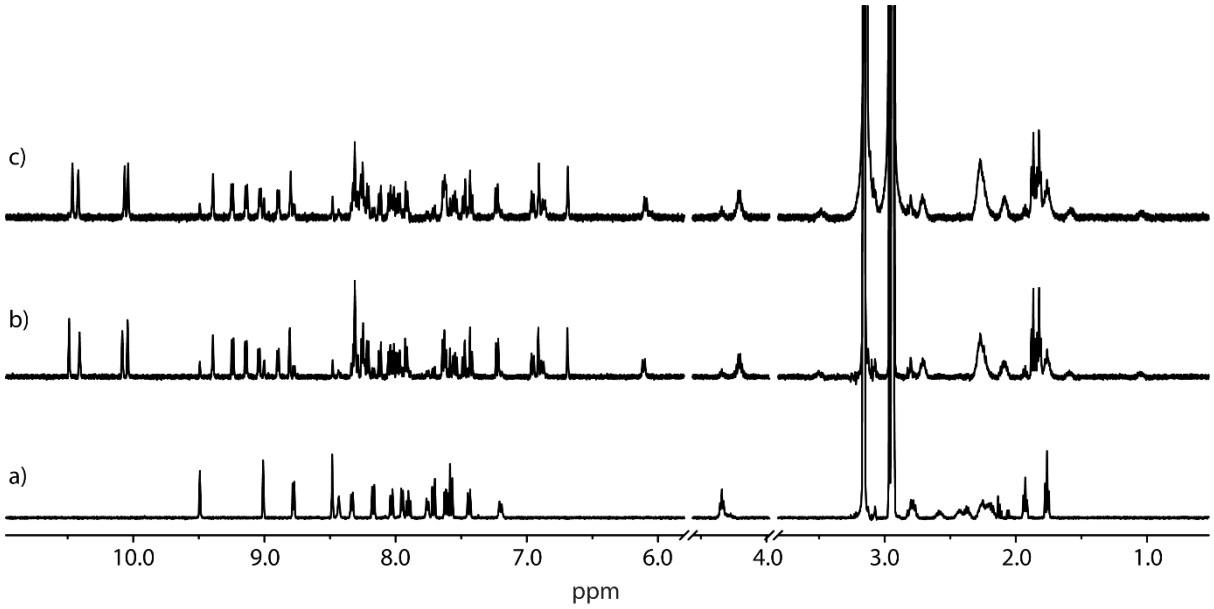

Figure S25. Partial ^{1}H NMR spectra (500 MHz/CD_3CN): a) 1:1 mixture of $[Pd_2\mathbf{L}^{\mathbf{A}}{}_4]^{4+}$ and $[Pd_2\mathbf{L}^{\mathbf{C}}{}_4]^{4+}$; b) 1:1 mixture of $[Pd_2\mathbf{L}^{\mathbf{A}}{}_4]^{4+}$ and $[Pd_2\mathbf{L}^{\mathbf{C}}{}_4]^{4+}$ heated for 24 h at 70 °C; c) *trans*-$[Pd_2(anti\text{-}\mathbf{L}^{\mathbf{A}})_4\mathbf{L}^{\mathbf{C}}{}_2]^{4+}$ (**3**) obtained by heated a 1:1:1 mixture of $\mathbf{L}^{\mathbf{A}}$, $\mathbf{L}^{\mathbf{C}}$ and $[Pd(CH_3CN)_4](BF_4)_2$ at 70 °C for 24 h, shown for comparison. Species distribution: b) **3**/$[Pd_2\mathbf{L}^{\mathbf{A}}{}_4]^{4+}$/$[Pd_2\mathbf{L}^{\mathbf{C}}{}_4]^{4+}$: 14:1.1:0.9; c) **3**/$[Pd_2\mathbf{L}^{\mathbf{A}}{}_4]^{4+}$/$[Pd_2\mathbf{L}^{\mathbf{C}}{}_4]^{4+}$: 14:1.2:1

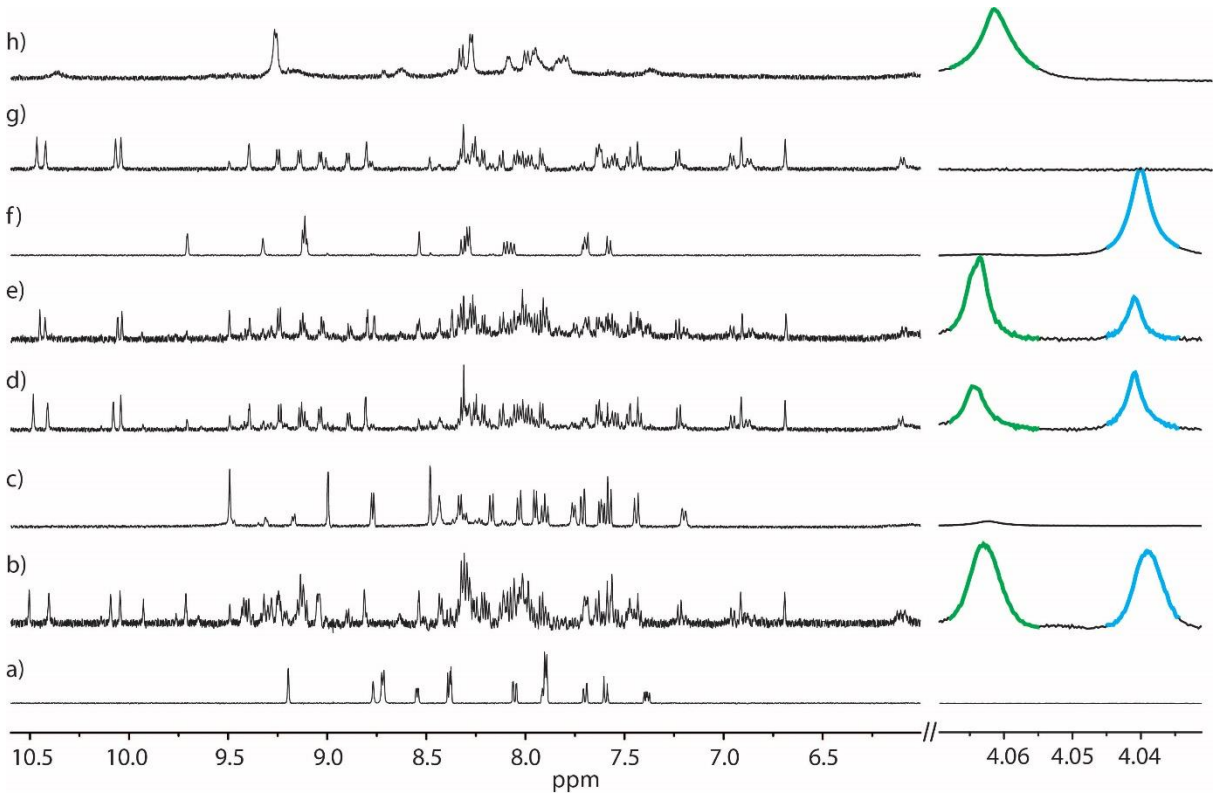

Figure S26. Partial ^{1}H NMR spectra (500 MHz/CD_3CN): a) 1:1:1 mixture of $\mathbf{L^A}$, $\mathbf{L^P}$ and $\mathbf{L^C}$. Note, $\mathbf{L^A}$ is not soluble in CD_3CN (present as a suspension); b) 1:1:1:1.5 mixture of $\mathbf{L^A}$, $\mathbf{L^P}$, $\mathbf{L^C}$ and $[Pd(CH_3CN)_4](BF_4)_2$ heated for 4 days at 70 °C; c) a 1:1:1 mixture of $[Pd_2\mathbf{L^A}_4]^{4+}$, $[Pd_2\mathbf{L^C}_4]^{4+}$ and $[Pd_3\mathbf{L^P}_6]^{6+}$/$[Pd_4\mathbf{L^P}_8]^{8+}$; d) a 1:1:1 mixture of $[Pd_2\mathbf{L^A}_4]^{4+}$, $[Pd_2\mathbf{L^C}_4]^{4+}$ and $[Pd_3\mathbf{L^P}_6]^{6+}$/$[Pd_4\mathbf{L^P}_8]^{8+}$ heated for 4 days at 70 °C; e) a 1:1:1 mixture of $[Pd_2\mathbf{L^A}_4]^{4+}$, $[Pd_2\mathbf{L^C}_4]^{4+}$ and $[Pd_3\mathbf{L^P}_6]^{6+}$/$[Pd_4\mathbf{L^P}_8]^{8+}$ heated for 1 day at 70 °C in the presence of 0.5 eq. Cl^- ions; f) *trans*-$[Pd_2(anti\text{-}\mathbf{L^A})_2\mathbf{L^C}_2]^{4+}$ (**3**); g) *cis*-$[Pd_2\mathbf{L^C}_2\mathbf{L^P}_2]^{4+}$ (**2**); h) *cis*-$[Pd_2\mathbf{L^A}_2\mathbf{L^P}_2]^{4+}$ (**1**). As can be observed, the combination of the three ligands $\mathbf{L^A}$, $\mathbf{L^P}$ and $\mathbf{L^C}$ or their homoleptic cages leads to a similar mixture where cage ***3*** is the major product. Addition of Cl^- ions in e) results in an increase in the formation of **1**. Species distribution: b) **3**/**2**/**1**/$[Pd_2\mathbf{L^A}_4]^{4+}$/$[Pd_2\mathbf{L^C}_4]^{4+}$: 2:0.9:1.2:0.2:0.17; d) **3**/**2**/**1**/$[Pd_2\mathbf{L^A}_4]^{4+}$/$[Pd_2\mathbf{L^C}_4]^{4+}$: 14:2:1.7:0.5:0.2; e) **3**/**2**/**1**/$[Pd_2\mathbf{L^A}_4]^{4+}$/$[Pd_2\mathbf{L^C}_4]^{4+}$: 14:2.8:6.6:4.1:1.5. (Colour code: green = **1**, blue = **2**).

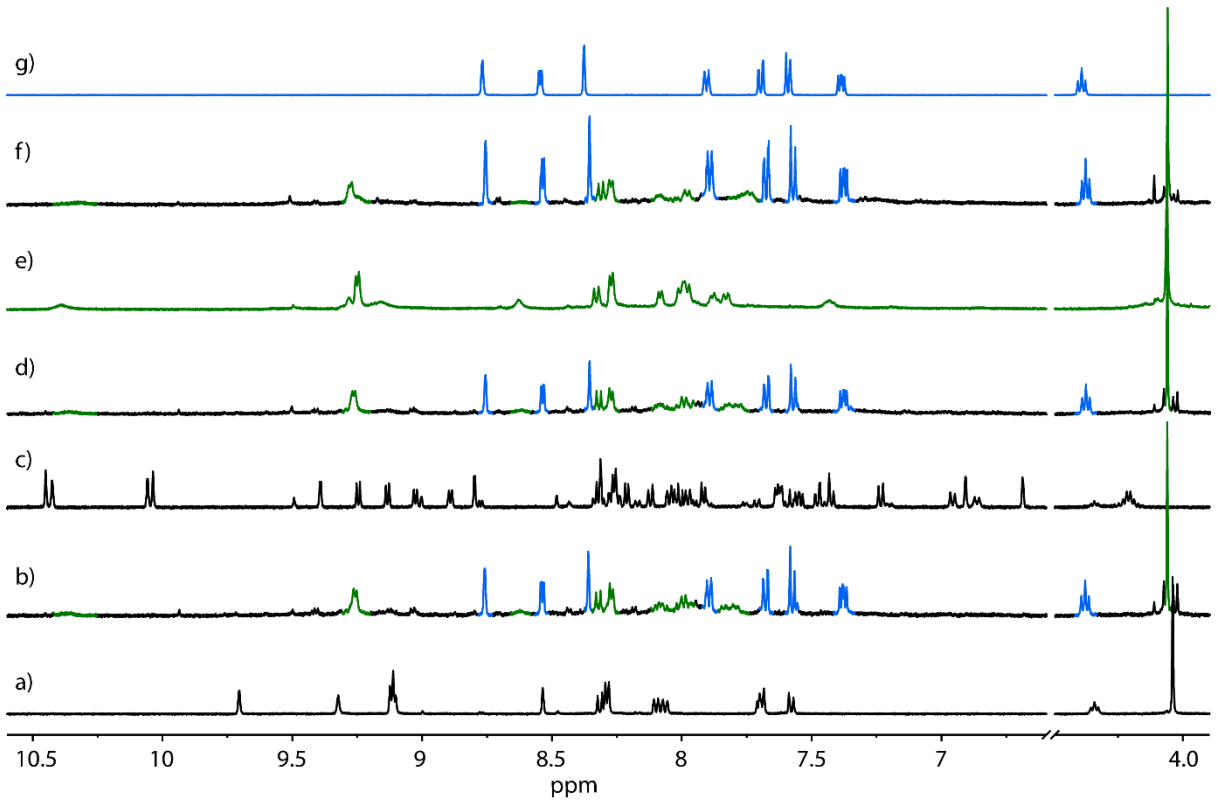

Figure S27. Partial ^{1}H NMR spectra (500 MHz/CD_3CN): a) *cis*-$[Pd_2\mathbf{L^C}_2\mathbf{L^P}_2]^{4+}$ (**2**); b) **2** + 2 equiv. of $\mathbf{L^A}$, heated for 6 h at 70 °C; c) *trans*-$[Pd_2(anti\text{-}\mathbf{L^A})_2\mathbf{L^C}_2]^{4+}$ (**3**); d) **3** + 2 equiv. of $\mathbf{L^P}$, heated for 6 h at 70 °C; e) *cis*-$[Pd_2\mathbf{L^A}_2\mathbf{L^P}_2]^{4+}$ (**1**); f) **1** + 2 equiv. of $\mathbf{L^C}$, heated for 6 h at 70 °C; g) $\mathbf{L^C}$. As can be

seen, the ^{1}H NMR signals corresponding to **1** (green colour) in spectra b) d) and f) are essentially identical to that in e). Colour code: blue: $\mathbf{L^C}$, green: **1**.

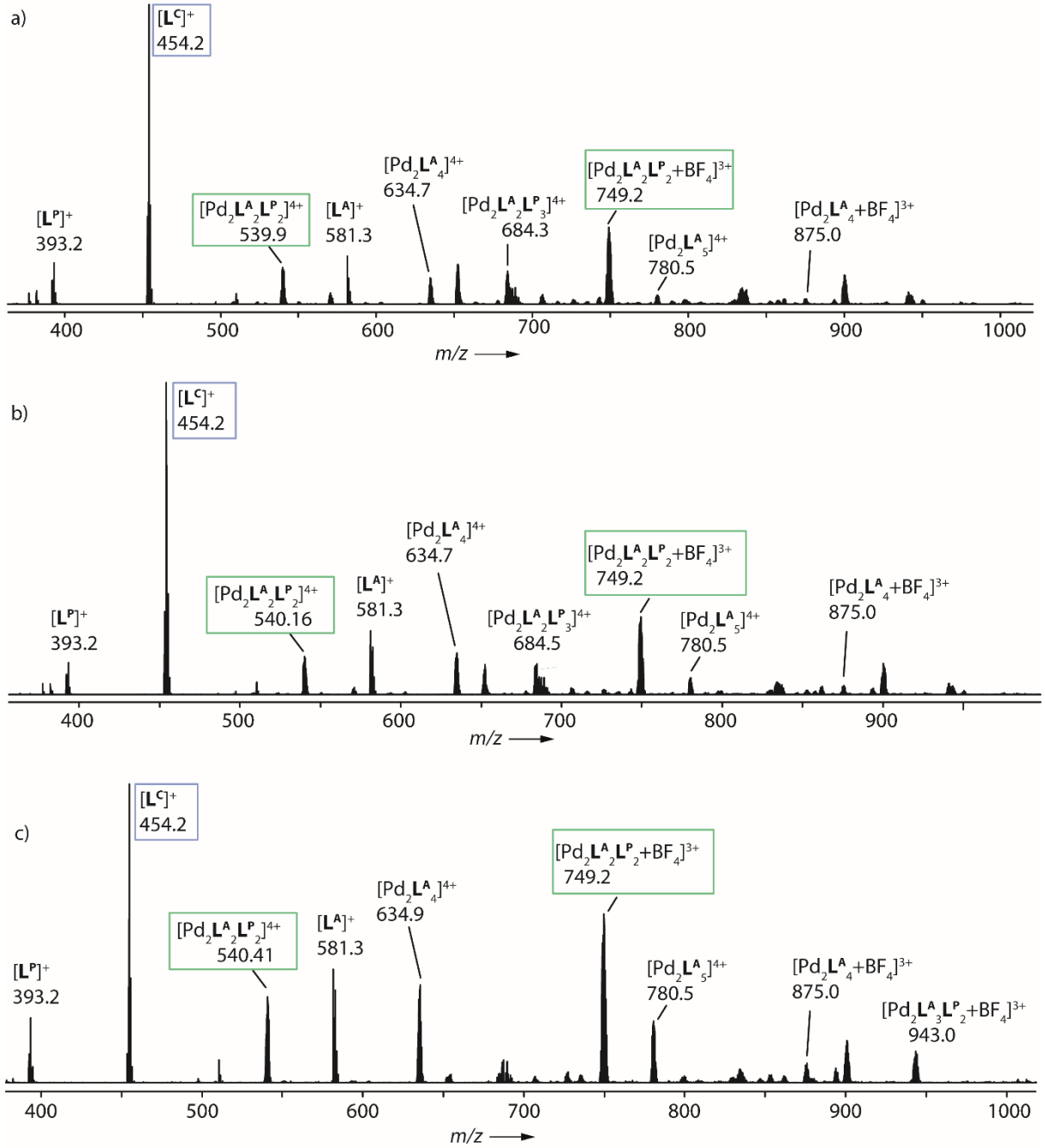

Figure S28. ESI-MS spectra obtained from the substitution reactions described in Figure S27; a) **2** + 2 equiv. of $\mathbf{L^A}$, heated for 6 h at 70 °C; b) **3** + 2 equiv. of $\mathbf{L^P}$, heated for 6 h at 70 °C; c) **1** + 2 equiv. of $\mathbf{L^C}$, heated for 6 h at 70 °C. As can be seen, the above spectra are essentially the same, indicating the same outcome in all three reactions; the selective assembly of **1** (and displacement of $\mathbf{L^C}$). The products as observed in the ^{1}H NMR spectrum (Figure S27) are highlighted in a box.

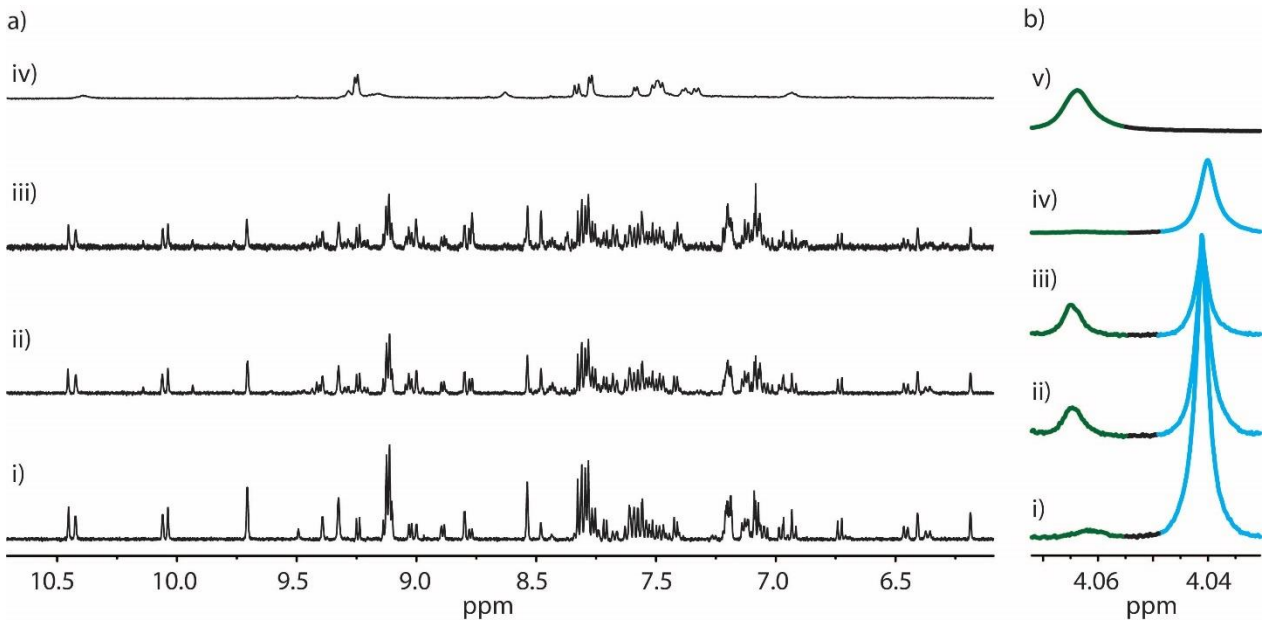

Figure S29. a) Partial ^{1}H NMR spectra (500 MHz/CD_3CN): i) unequilibrated 1:1 mixture of **2** and **3**.; ii) 1:1 mixture of **2** and **3** heated at 70 °C for 24 h; iii) 1:1 mixture of **2** and **3** + 0.5 eq. Cl^- heated at 70 °C for 48 h; iv) **1**. b) Partial ^{1}H NMR spectra (500 MHz/CD_3CN) showing only the region of the OMe signals (blue = **2**, green = **1**): i) unequilibrated 1:1 mixture of **2** and **3**; ii) 1:1 mixture of **2** and **3** heated at 70 °C for 24 h; iii) 1:1 mixture of **2** and **3** + 0.5 eq. Cl^- heated at 70 °C for 48 h; iv) **2**; v) **1**. From the NMR stacks in a) it is difficult to examine the cage-to-cage transformation of **2** and **3** to **1**. In b), it can be see that **1** is formed by the appearance of the OMe signals (coloured green). Ratio of **1**/**2**/**3**; ii) 1.6 / 9.4 / 10; iii) 4.8 / 11.0 / 10.

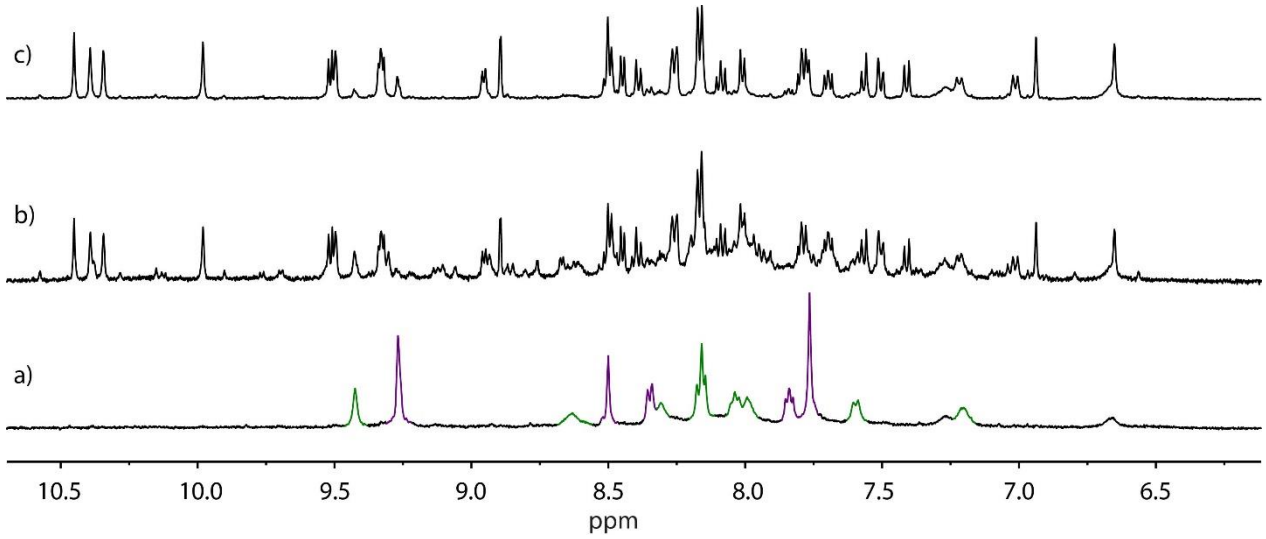

Figure S30. a) Partial ^{1}H NMR spectra (500 MHz/DMSO): a) unequilibrated 1:1 mixture of $[Pd_2\mathbf{L}^{\mathbf{A}}{}_4]^{4+}$ (green) and $[Pd_2\mathbf{L}^{\mathbf{C}}{}_4]^{4+}$ (purple); b) a) heated at 70 °C for 24 h; c) **3**. The cage to cage rearrangement of $[Pd_2\mathbf{L}^{\mathbf{A}}{}_4]^{4+}$ and $[Pd_2\mathbf{L}^{\mathbf{C}}{}_4]^{4+}$ to **3** is complete within 24 h. The same experiment between $[Pd_2\mathbf{L}^{\mathbf{A}}{}_4]^{4+}$ and $[Pd_4\mathbf{L}^{\mathbf{P}}{}_8]^{8+}$ to give **1** required 288 h (12 days).[1] The slower kinetics in the latter case explains why the meta-stable cage **3** is the favoured product in the experiments described in figure S26.

4. Deconstruction experiments

Deconstruction experiments were performed by adding 8 equivalents of pyridine-d_5 in CD_3CN (3.36 M) to a CD_3CN solution of the respective cage and allowing the mixture to equilibrate for 24 h at room temperature.

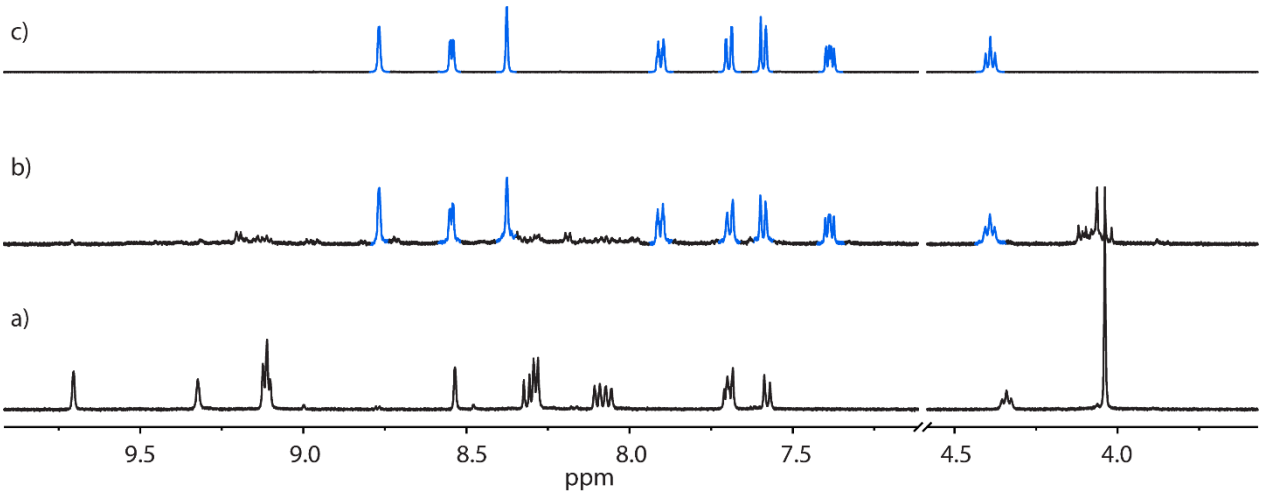

Figure S31. Partial ^{1}H NMR spectra (500 MHz/CD_3CN/25 °C) of a) Cage **2**; b) A mixture of **2** + 8 equivalents of pyridine allowed to equilibrate for 24 h; c) $\mathbf{L^C}$, shown for comparison. As can be seen, the presence of signals corresponding to $\mathbf{L^C}$ (coloured blue) and complete absence of the original signals of **2** in b) indicates complete decomposition of the cage.

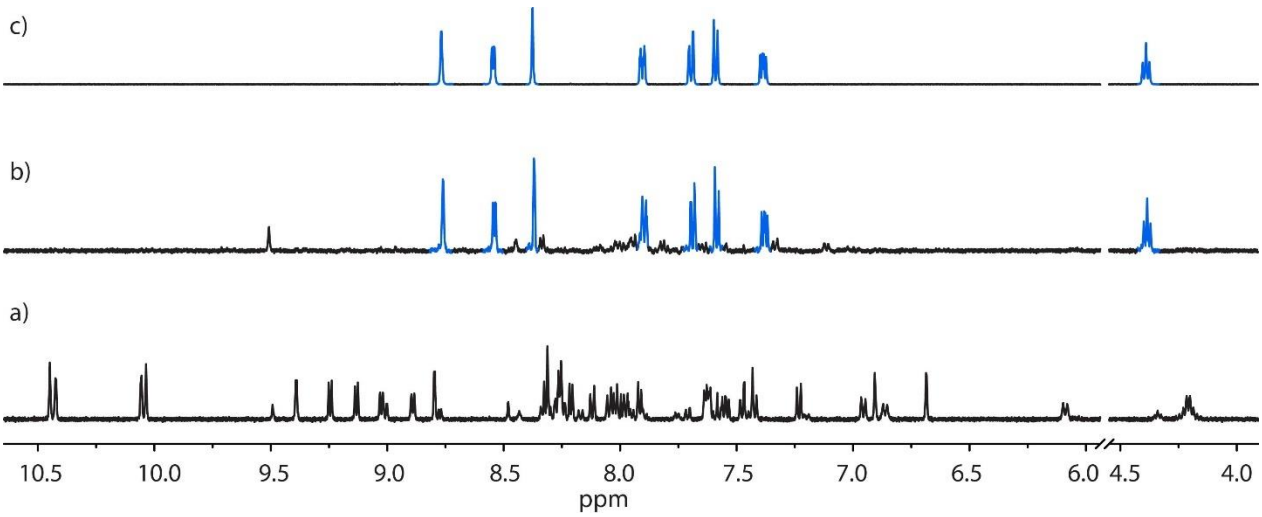

Figure S32. Partial ^{1}H NMR spectra (500 MHz/CD_3CN/25 °C) of a) Cage **3**; b) A mixture of **3** + 8 equivalents of pyridine allowed to equilibrate for 24 h; c) $\mathbf{L^C}$, shown for comparison. As can be seen, the presence of signals corresponding to $\mathbf{L^C}$ (coloured blue) and complete absence of the original signals of **3** in b) indicates complete decomposition of the cage.

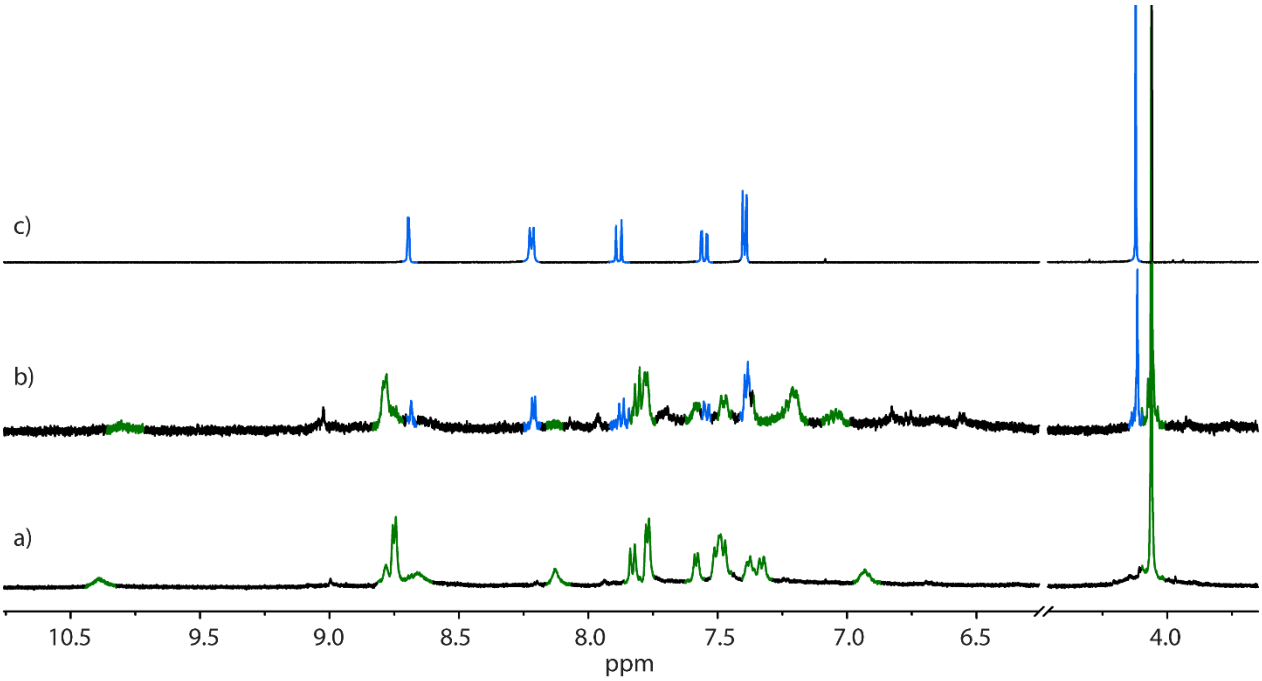

Figure S33. Partial ^{1}H NMR spectra (500 MHz/CD_3CN/25 °C) of a) Cage **1**; b) A mixture of **1** + 8 equivalents of pyridine allowed to equilibrate for 24 h; c) $\mathbf{L^P}$, shown for comparison. As can be seen, the presence of the original signals of **1** (coloured green) in b) indicates incomplete decomposition of the cage ($\mathbf{L^C}$ = blue).

5. X-ray crystallography

Table S1 X-ray experimental data for $\mathbf{L^C}$, **2** and **3**.

Compound	$\mathbf{L^C}$	**2**	**3**
CCDC number	1537048	1537049	1537050
Empirical formula	$C_{32}H_{27}N_3$	$C_{394}H_{356}B_8F_{32}N_{20}O_{10}Pd_4$	$C_{322}H_{292}B_8F_{32}N_{30}O_7Pd_4$
Formula weight	453.56	6651.05	5813.92
Crystal system	Monoclinic	triclinic	monoclinic
Space group	$P2_1/n$	P-1	Cc
a (Å)	13.3224(12)	23.0970(9)	32.1429(8)
b (Å)	8.9898(15)	28.8761(10)	20.0109(5)
c (Å)	21.046(2)	29.6965(11)	27.5787(11)
α (°)	90	70.491(2)	90
β (°)	102.097(10)	74.525(2)	118.968(3)
γ (°)	90	68.874(2)	90
Volume (Å^3)	2464.6(5)	17171.0(12)	15519.5(9)
Z	4	2	2
Density (calc.) (Mg/m^3)	1.222	1.286	1.244
Absorption coefficient (mm^{-1})	0.072	2.320	2.494
F(000)	960	6904	6004
Crystal size (mm^3)	0.22 x 0.20 x 0.14	0.30 x 0.11 x 0.06	0.17 x 0.15 x 0.05
θ range for data collection (°)	2.472 to 24.710	2.259 to 68.244	2.710 to 66.897
Reflections collected	10892	434264	54995
Observed reflections [R(int)]	4115 [0.0702]	62570 [0.0900]	19034 [0.0489]
Goodness-of-fit on F^2	1.006	1.061	1.019
R_1 [I>2σ(I)]	0.0562	0.1247	0.0588
wR_2 (all data)	0.1112	0.3533	0.1667
Largest diff. peak and hole (e.Å-3)	0.194 and -0.206	2.472 and -2.093	1.279 and -0.728
Data / restraints / parameters	4115 / 0 / 317	62570 / 15690 / 5257	19034 / 3479 / 1847

5.1. Crystal structure of L^C

A single crystal was mounted in NVH oil on a nylon loop. X-ray diffraction data were collected at 100(2) K on an Oxford X-Calibur single crystal diffractometer (λ = 0.71073 Å). Data sets were corrected for absorption using a multi-scan method, and structures were solved by direct methods using SHELXS[6] and refined with SHELXL[7] using full-matrix least-squares routines on F^2 and ShelXle[8] as a graphical user interface. All non-hydrogen atoms were refined anisotropically and hydrogen atoms were included as invariants at geometrically estimated positions.

5.2. Crystal structure of 2

Crystals of **2** are extremely solvent dependant and immediately cracked after being removed from mother liquor. To avoid (full) collapse of the crystal lattice due to loss of organic solvents, the crystals were pipetted from mother liquor into a drop of NVH oil, from where they were very quickly mounted on nylon loops and immediately flash-cooled in liquid nitrogen.

X-ray diffraction data were collected on a Bruker D8 venture equippend with an Incoatec microfocus source (Iμs 2.0) using Cuk_α radiation and an Oxford Cryostream 800 at 100(2) K. Only one crystal of a series had sufficient scattering power up to d = 0.83 Å. Data integration and reduction were undertaken with SAINT and XPREP.[9] Multi-scan empirical absorption correction was applied to the data using SADABS.[9, 10] The structure was solved by intrinsic phasing/direct methods using SHELXT[11] and refined with SHELXL[7] using 24 cpu cores for full-matrix least-squares routines on F^2 and ShelXle[8] as a graphical user interface

*5.2.1. Specific refinement details for **2***

The heteroleptic structure crystallizes in the triclinic space group $P\bar{1}$ with two, almost identical molecules of the cage, in the asymmetric unit. Due to the very high resolution of approximately d = 0.83 Å of the diffraction experiment, we were able to locate and model all eight BF_4^- counter ions, two acetone and 26 benzene molecules in the residual density. The structure was grouped into residues as shown in the following table. This is not only required in order to use advanced macromolecular refinement protocols, but also increases clarity in the SHELX .res file.

Ligand	Residue class	Occurrence	Residue numbers
Pd^{2+}	PD	2	31, 32 (each containing two Pd^{2+} ions)
$\mathbf{L^P}$	WB2	4	3,4,7,8
$\mathbf{L^C}$	WB3	4	1,2,5,6
BF_4^-	BF4	8	11- 18
Acetone	ACN	2	19, 20
Benzene	BEN	26	41 - 67

Advanced refinement techniques commonly applied for macromolecular structures were employed to generate a molecular model and increase robustness of the refinement. Stereochemical restraints for all organic ligands (residue classes WB2 and WB3) and solvents (residue classes BEN, ACN) of the structure were generated by the GRADE program using the GRADE Web Server (http://grade.globalphasing.org) and applied in the refinement. A GRADE dictionary for SHELXL contains target values and standard deviations for 1.2-distances (DFIX) and 1.3-distances (DANG), as well as restraints for planar groups (FLAT). The refinement of ADP's for non-hydrogen atoms was enabled by using the new rigid bond restraint (RIGU) in the SHELXL 2016 program in combination with SIMU restraints. Stereochemincal restraints for BF_4^- counter ion were manually derived from the CSD using the Mogul software. For building an initial model, the structural modeling process was enhanced by using DSR.[12]

Ten of the 26 solvent benzene molecules were modelled as fully occupied, while the remaining 16 were disordered and modelled as two parts/conformers over two positions. Due to crystallographic symmetry, the disordered benzene molecules form a solvent channel through the unit cell. Two parts/conformations were also introduced for two of the highly flexible hexyl chains of ligand C (residue WB3) pointing into the benzene solvent channel and three of the BF_4^- counter ions. Occupancy of disordered parts were kept fixed at 50 %. The same atom names are used for different disorder components, which thereby only differ in their part numbers. Hydrogen atoms were included as invariants at geometrically estimated positions. The TABS keyword behind the ACTA instruction in SHELXL (Sheldrick, 2016) was employed to generate the CIF and prevent clashes in CHEKCIF routines due to identical atom names.

5.3. Crystal structure of 3

A single crystal was mounted in NVH oil on a nylon loop. X-ray diffraction data were collected on a Rigaku Oxford Diffraction Synergy-S equipped with PhotonJet-S using Cuk_α radiation, a HyPix-6000HE detector and an Oxford Cryostream 800 at 100(2) K. Data integration and reduction were undertaken in CrystalisPro. Gaussian absorption

correction was applied to the data using CrystalisPro. The structure was solved by intrinsic phasing/direct methods using SHELXT[11] and refined with SHELXL[7] using 24 cpu cores for full-matrix least-squares routines on F^2 and ShelXle[8] as a graphical user interface.

*5.3.1. Specific refinement details for **3***

The heteroleptic structure was solved in the monoclinic space group *Cc* and contains one cage in the asymmetric unit. Due to the very high resolution of approximately d = 0.83 Å of the diffraction experiment, we were able to also locate and successfully model all four BF_4^- counter ions and 1.5 diisopropylether solvent molecules. The structure was grouped into residues as shown in the following table. This is not only required in order to use advanced macromolecular refinement protocols, but also increases clarity in the SHELX .res file.

Fragment	Residue class	Occurrence	Residue number(s)
Pd^{2+}	PD	1	1 (containing two Pd^{2+} ions)
L^A	WB1	2	3,4
L^C	WB3	2	2,3
BF_4^-	BF4	4	8-14
Diisopropylether	DIP	2	6,7

Advanced refinement techniques commonly applied for macromolecular structures were employed to generate a molecular model and increase robustness of the refinement. Stereochemical restraints for all organic ligands (residue classes WB2 and WB3) and solvents (residue classes BEN, ACN) of the structure were generated by the GRADE program using the GRADE Web Server (http://grade.globalphasing.org) and applied in the refinement. A GRADE dictionary for SHELXL contains target values and standard deviations for 1.2-distances (DFIX) and 1.3-distances (DANG), as well as restraints for planar groups (FLAT). The refinement of ADP's for non-hydrogen atoms was enabled by using the new rigid bond restraint (RIGU) in the SHELXL 2016 program in combination with SIMU restraints. Stereochemical restraints for BF_4^- counter ion were manually derived from the CSD using the Mogul software. For building an initial model, the structural modeling process was enhanced by using DSR.[12]

Hexyl chains of **L^C** (residue WB3) are very flexible and required additional similarity restraints (SADI) for 1.3 carbon-carbon distances. The structure was refined as two component twin using [1 0 0 0 1 0 0 -1] as twin law yielding 0.604(9) volume percent for the first twin domain. The contribution of the electron density associated with disordered solvent molecules, which could not be modelled with discrete atomic positions were handled using the SQUEEZE[13] routine in PLATON.[14,15] Solvent masks (.fab files) generated by PLATON were included in the SHELXL refinement via the ABIN instruction in order to leave the original structure factors untouched.

The refined enantiopure distinguishing parameter after Parsons[16] [z =-0.019(6)] strongly indicates that an enantiopure crystal was measured. Hence the chirality of the measured structure can be derived. It shows the *M,M* configuration of the 'figure-eight' motif. We nevertheless have to assume that there is a dynamic racemic mixture of cages in solution, as there was no external chiral information provided to favor the assembly of one enantiomeric cage over the other. The the enantiopure distinguishing parameter calculation from a twin refinement with additional application of a squeeze solvent mask, however, carries a degree of uncertainty.

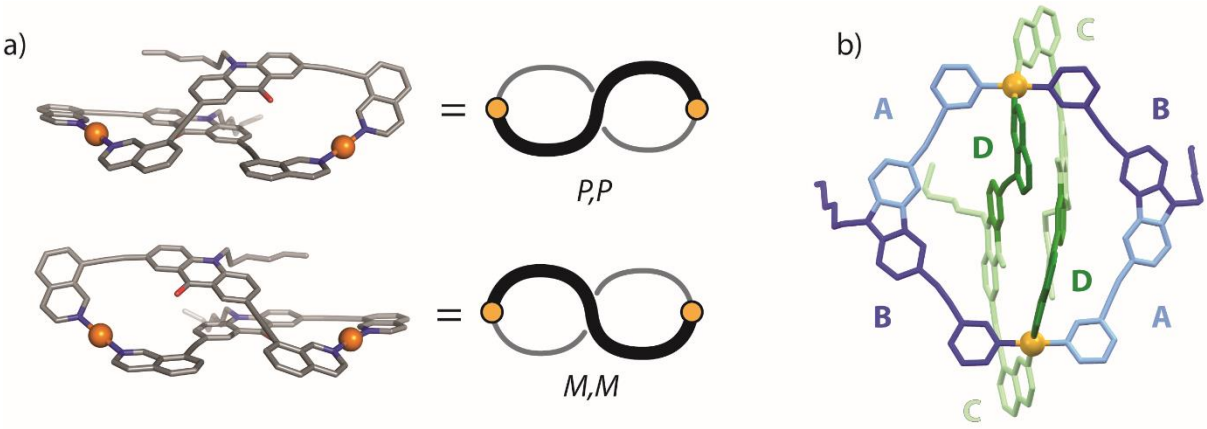

Figure S34. a) The two enantiomers of the 'figure-eight' motif of ligand **L^A** in **3**. The figure eight conformation is comprised of two equidirectional helices *P,P* (top) or *M,M* (bottom); b) The structural symmetry of **3** (point group = *S2*) denoted by colours and letters (**L^C**: A, B (blue); **L^A**: C, D (green)). Both **L^A** and **L^C** have lost symmetry which leads to the two-fold splitting in the ^{1}H NMR spectrum.

5.4. Thermal ellipsoid plots

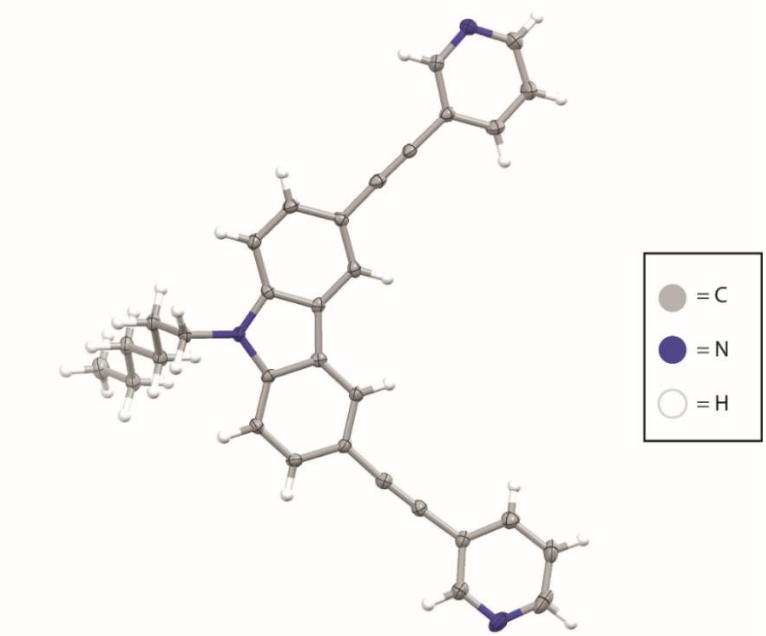

Figure S35. The asymmetric unit of the X-ray structure of $\mathbf{L}^{C}$, with all non-hydrogen atoms shown as ellipsoids at the 50% probability level.

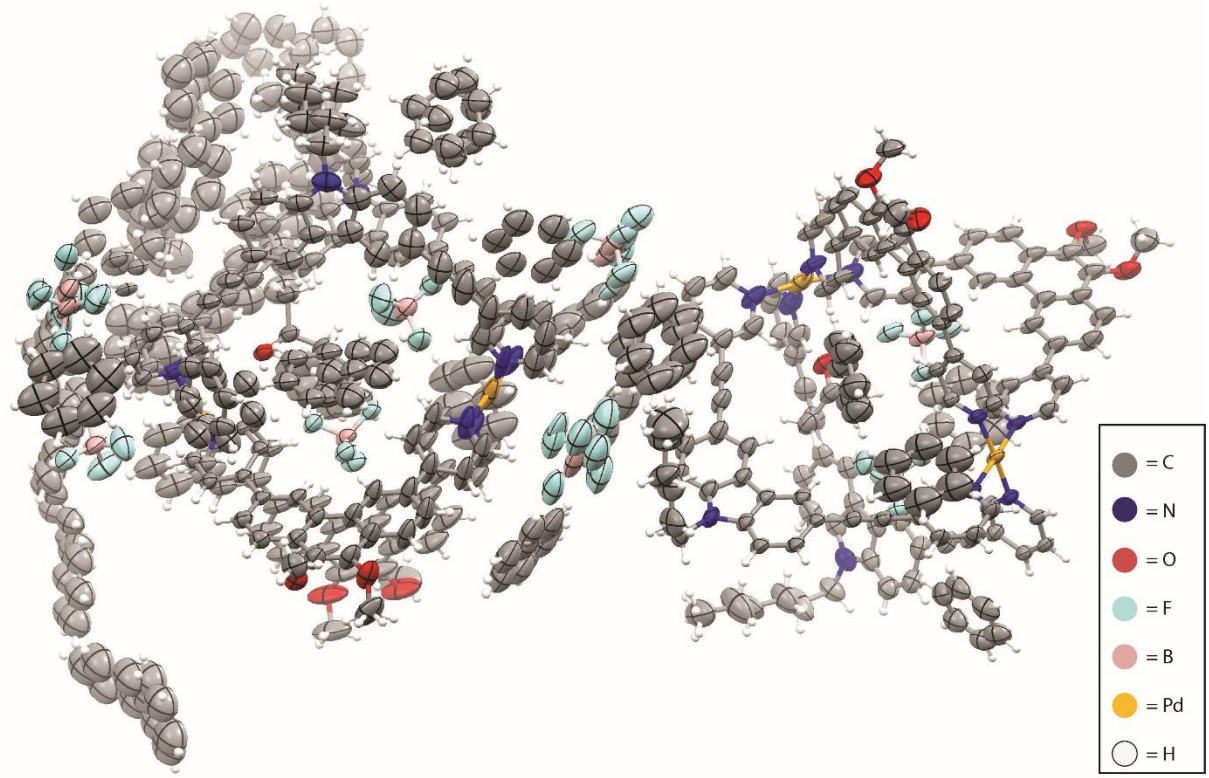

Figure S36. The asymmetric unit of the X-ray structure of **2**, with all non-hydrogen atoms shown as ellipsoids at the 50% probability level.

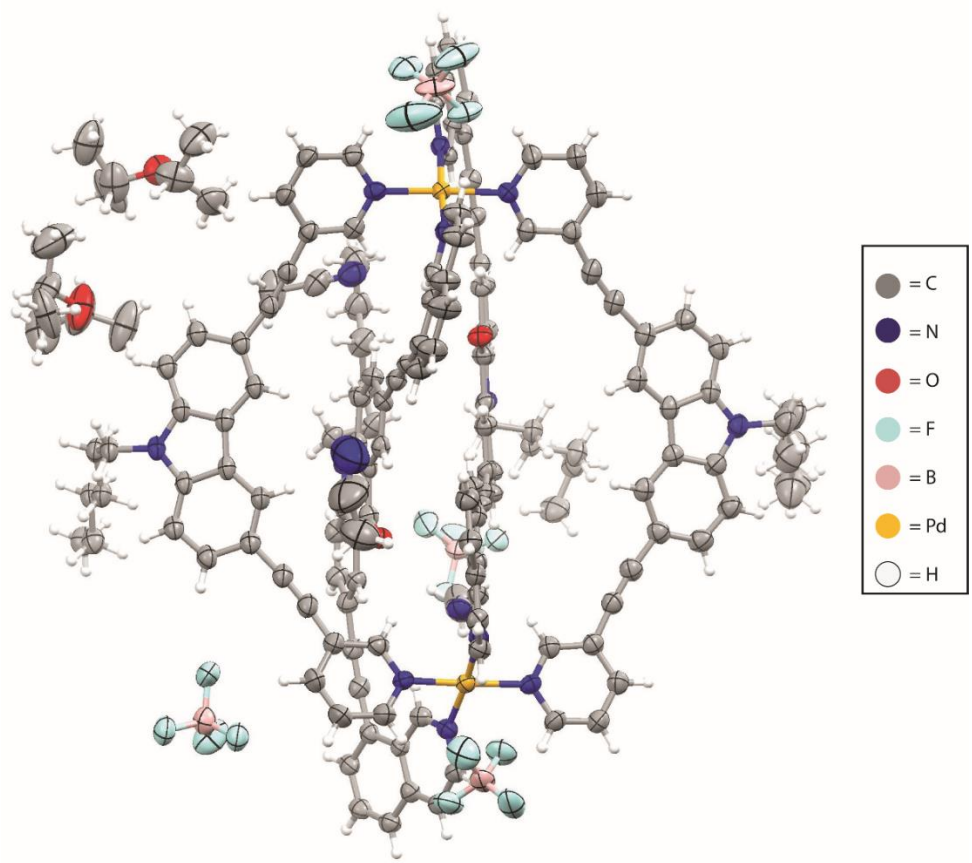

Figure S37. The asymmetric unit of the X-ray structure of **3**, with all non-hydrogen atoms shown as ellipsoids at the 50% probability level.

6. Structural comparisons

*6.1.1. Comparison of cages **1** – **3***

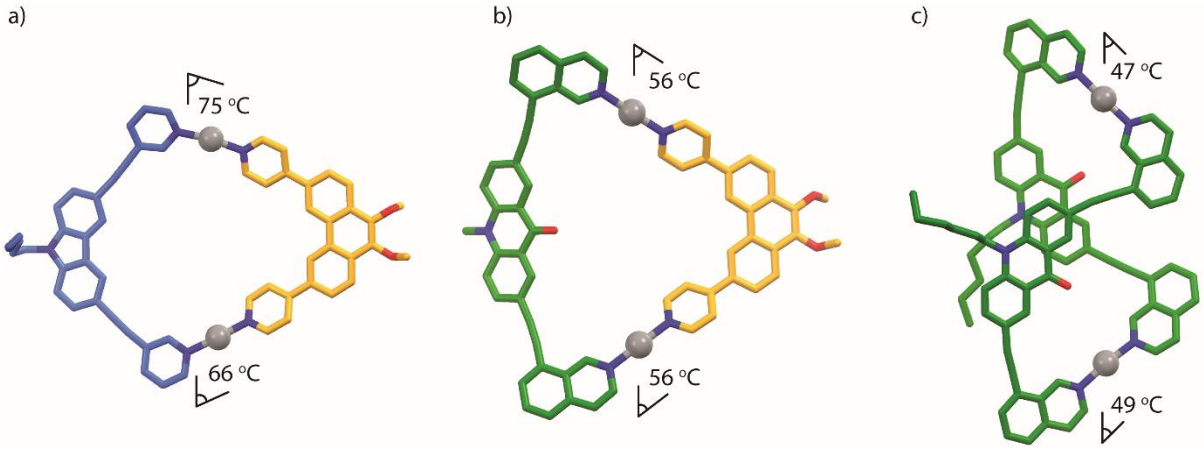

Figure S38. A comparison of the Pd planes in heteroleptic cage structures **1** – **3**, with only two of the four ligands shown. The Pd planes were determined by measuring the Pd···Pd···N angle from the respective crystal structure (**2** and **3**) or DFT model (**1**); a) **2**; b) **1**; c) **3**.

6.1.2. *Comparison of cages containing* $\mathbf{L^C}$

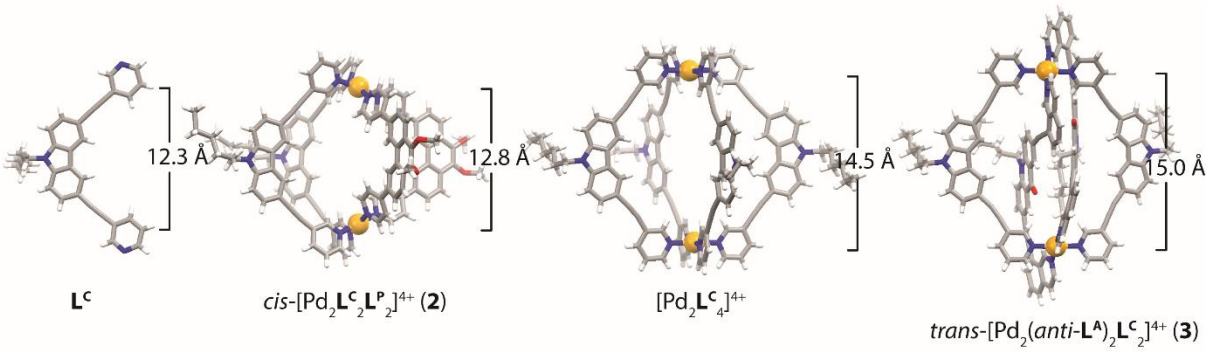

Figure S39. A comparison of the binding distance (N···N distance) for cages composed of $\mathbf{L^C}$. All of the lengths are derived from the respective crystal structures. Note: for the free ligand (left), the distance was estimated based on the rotation of the pyridine ring.

7. UV-Vis spectroscopy

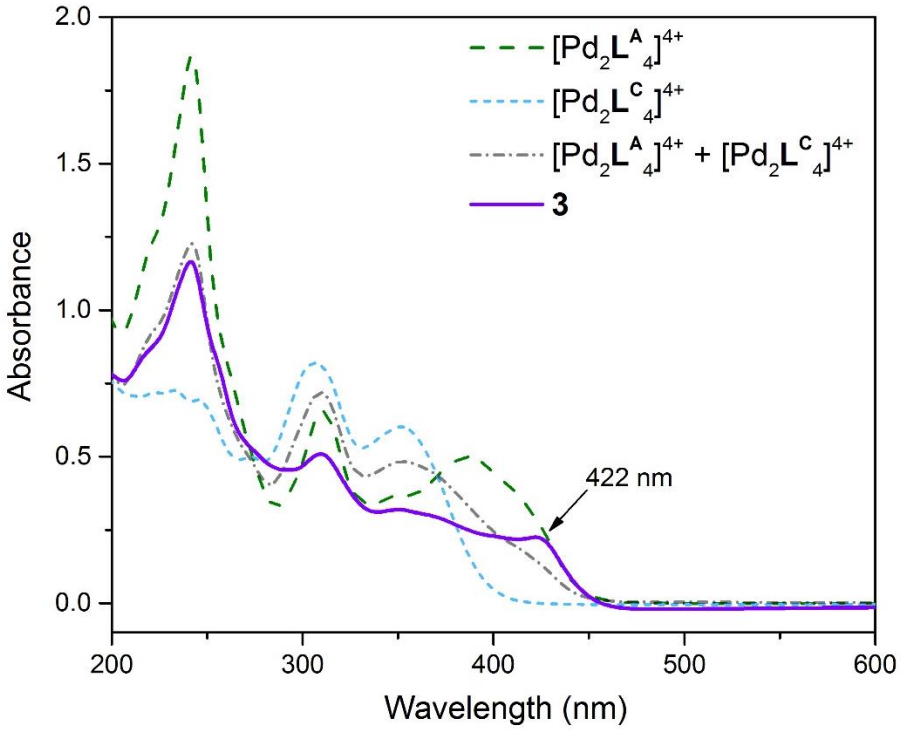

Figure S40. UV-Vis spectra measured in CH_3CN at 25 °C: $[Pd_2\mathbf{L^A}_4]^{4+}$ ([C] = 4.2 μL); $[Pd_2\mathbf{L^C}_4]^{4+}$ ([C] = 4.2 μL); 1:1 unequilibrated mixture of $[Pd_2\mathbf{L^A}_4]^{4+}$ and $[Pd_2\mathbf{L^C}_4]^{4+}$ ([C] = 2.1+2.1 μL); cage **3** ([C] = 4.2 μL). The spectrum corresponding to heteroleptic cage **3** (purple line) possesses an absorption band at 422 nm (due to the $\mathbf{L^A}$···$\mathbf{L^A}$ π – stacking interaction present in **3**) which is absent in the 1:1 unequilibrated mixture of homoleptic cages (grey dashed line). Cuvette path length = 1cm.

8. References

1 W. M. Bloch, Y. Abe, J. J. Holstein, C. M. Wandtke, B. Dittrich and G. H. Clever, *J. Am. Chem. Soc.*, 2016, **138**, 13750–13755.

2 R. Zhu, J. Lübben, B. Dittrich and G. H. Clever, *Angew. Chem. Int. Ed.*, 2015, **54**, 2796–2800.

3 C. Klein, C. Gütz, M. Bogner, F. Topić, K. Rissanen and A. Lützen, *Angew. Chem. Int. Ed.*, 2014, **53**, 3739–3742.

4 M. J. Frisch, G. W. Trucks, H. B. Schlegel, G. E. Scuseria, M. A. Robb, J. R. Cheeseman, G. Scalmani, V. Barone, B. Mennucci, G. A. Petersson, H. Nakatsuji, M. Caricato, X. Li, H. P. Hratchian, A. F. Izmaylov, J. Bloino, G. Zheng, J. L. Sonnenberg, M. Hada, M. Ehara, K. Toyota, R. Fukuda, J. Hasegawa, M. Ishida, T. Nakajima, Y. Honda, O. Kitao, H. Nakai, T. Vreven, J. A. Montgomery Jr., J. E. Peralta, F. Ogliaro, M. J. Bearpark, J. Heyd, E. N. Brothers, K. N. Kudin, V. N. Staroverov, R. Kobayashi, J. Normand, K. Raghavachari, A. P. Rendell, J. C. Burant, S. S. Iyengar, J. Tomasi, M. Cossi, N. Rega, N. J. Millam, M. Klene, J. E. Knox, J. B. Cross, V. Bakken, C. Adamo, J. Jaramillo, R. Gomperts, R. E. Stratmann, O. Yazyev, A. J. Austin, R. Cammi, C. Pomelli, J. W.

Ochterski, R. L. Martin, K. Morokuma, V. G. Zakrzewski, G. A. Voth, P. Salvador, J. J. Dannenberg, S. Dapprich, A. D. Daniels, Ö. Farkas, J. B. Foresman, J. V Ortiz, J. Cioslowski and D. J. Fox, 2009.

5 K. Suzuki, M. Kawano, M. Fujita, *Angew. Chem. Int. Ed.* **2007**, *46*, 2819–2822.

6 G. Sheldrick, *Acta Crystallogr. Sect. A*, 2008, **64**, 112–122.

7 G. M. Sheldrick, *Acta Crystallogr. Sect. C*, 2015, **71**, 3–8.

8 C. B. Hubschle, G. M. Sheldrick and B. Dittrich, *J. Appl. Crystallogr.*, 2011, **44**, 1281–1284.

9 A. Bruker-Nonius SAINT, SADABS and XPREP, 2013.

10 G. M. Sheldrick, *No Title*, SADABS, Universität Göttingen, Germany, 2000.

11 G. M. Sheldrick, *Acta Crystallogr. Sect. A*, 2015, **71**, 3–8.

12 D. Kratzert, J. J. Holstein and I. Krossing, *J. Appl. Crystallogr.*, 2015, **48**, 933–938.

13 A. Spek, *Acta Crystallogr. Sect. C*, 2015, **71**, 9–18.

14 A. L. Spek, Vol. 20, PLATON, a multipurpose crystallographic tool, Utrecht University, Utrecht, The Netherlands, 2001.

15 A. Spek, *Acta Crystallogr. Sect. D*, 2009, **65**, 148–155.

16 S. Parsons, H. D. Flack and T. Wagner, *Acta Crystallogr. Sect. B*, 2013, **69**, 249–259.